www.sciencemag.org/cgi/content/full/326/5949/144/DC1

Supporting Online Material for

Genome-Wide RNAi Screen Identifies Letm1 as a Mitochondrial Ca^{2+}/H^{+} Antiporter

Dawei Jiang, Linlin Zhao, David E. Clapham*

*To whom correspondence should be addressed. E-mail: dclapham@enders.tch.harvard.edu

Published 2 October 2009, *Science* **326**, 144 (2009)
DOI: 10.1126/science.1175145

This PDF file includes:

SOM Text
Materials and Methods
Figs. S1 to S9
Tables S1 to S3
References

Supporting Online Material (SOM)

Supplementary Text and Discussion

The free energy of mitochondrial respiration drives ATP synthesis; this energy is stored as an H^+ gradient across the inner mitochondrial membrane (IMM) created primarily by H^+ extrusion via the electron transport chain (ETC). The H^+ gradient that establishes the normally large negative membrane potential (~-180 mV) across the IMM is a significant driving force for Ca^{2+} entry. Mitochondrial Ca^{2+} uptake occurs via tightly regulated channels and transporters. For example, the mitochondrial Ca^{2+} uniporter (MCU) is mediated at least in part by a highly Ca^{2+}-selective conductance (MiCa; (*1, 2*)). Increases in matrix $[Ca^{2+}]$ enhance the activities of ATP synthase and enzymes in the tricarboxylic acid cycle, thus stimulating ATP production rates(*3, 4*). In turn, MCU/MiCa rapidly depolarizes the mitochondria and reduces Ca^{2+} entry, but may also abrogate the driving force for H^+ entry and ATP synthase function. The evidence suggests that Na^+/Ca^{2+}, Ca^{2+}/H^+, and other exchangers regulate mitochondrial Ca^{2+} homeostasis(*5-8*). If homeostatic mechanisms fail, high levels of matrix Ca^{2+} activate the mitochondrial permeability transition pore to induce necrotic or apoptotic cell death(*9, 10*). We set out to identify the genes that mediate Ca^{2+} flux across the mitochondrial inner membrane.

Simultaneous measurement of $[Ca^{2+}]_{mito}$ and $[H^+]_{mito}$ using pericam

Mt-pericam, a mitochondrial matrix-targeted (fig. S1A), circularly-permuted green fluorescent protein fused to calmodulin and its target peptide M13(*11*). Pericam emission due to excitation at 405 nm is sensitive to changes in $[Ca^{2+}]$ while emission in response to excitation at 488 nm reports changes in pH. Pericam can be used for simultaneous Ca^{2+} and H^+ detection (fig. S1B), its K_D and pKa ideal for measuring mitochondrial Ca^{2+} and H^+ concentrations ($[Ca^{2+}]_{mito}$ and $[H^+]_{mito}$; fig. S1C; (*11*)). In resting S2 cells stably expressing mitochondrial-targeted pericam, application of the H^+ ionophore, FCCP (carbonyl cyanide p-trifluoromethoxyphenylhydrazone) dramatically increased $[H^+]_{mito}$ with no immediate change in $[Ca^{2+}]_{mito}$ (fig. S2A). To induce changes in $[Ca^{2+}]_{cyto}$, thapsigargin was employed. Thapsigargin blocks SERCA pumps to deplete ER Ca^{2+} stores and activate plasma membrane Ca^{2+}-selective CRAC channels (*Olf186-F* in *Drosophila*; *Orai* in mammalian cells; (*12, 13*)). A thapsigargin-induced, sustained cytoplasmic Ca^{2+} ($[Ca^{2+}]_{cyto}$) elevation in S2 cells triggered not only mitochondrial Ca^{2+} uptake, but also mitochondrial H^+ extrusion (fig. S2B). Following FCCP application, $[H^+]_{mito}$ increased well above baseline without significantly affecting $[Ca^{2+}]_{mito}$.

Histamine receptor (phospholipase C-coupled H1) activation in HeLa cells transiently increased $[Ca^{2+}]_{cyto}$, which correlated with mitochondrial H^+_{mito} efflux, and a delayed $[Ca^{2+}]_{cyto}$ decline (at t > ~100 s) coinciding with H^+ entry (fig. S6). High $[Ca^{2+}]_{mito}$ correlated with H^+ influx into the mitochondria only at the lower $[Ca^{2+}]_{cyto}$ (fig. S6B,C; t >170 s), arguing that H^+ transport is not secondary to $[Ca^{2+}]_{mito}$ alone, but rather the Ca^{2+} gradient across the IMM. Increasing bath $[Ca^{2+}]$ from 2 mM to 10 mM prolonged the $[Ca^{2+}]_{cyto}$ elevation phase and prevented the late H^+_{mito} influx. The experiments confirmed mt-pericam's suitability for simultaneous Ca^{2+} and H^+ measurements in intact mammalian cells and suggest mitochondrial H^+ transport was not secondary to $[Ca^{2+}]_{mito}$ alone, but rather the Ca^{2+} gradient across the IMM.

The identification of *Letm1* from a genome-wide RNAi screen
Although mitochondrial respiration has been little studied in flies, RNA interference (RNAi) screens of *Drosophila* S2 cells have been an especially robust method for unbiased identification of genes when used with a reliable reporter. Reasoning that it was likely that mitochondrial mechanisms have been relatively well preserved in evolution, we conducted a *Drosophila* RNAi screen.

In order to cover genes encoding proteins of different turnover rates, 2 independent screens were performed. In each screen, 2 sets of sixty-two 384-well microplates containing the entire dsRNA collection were incubated with S2 cells for 3 or 5 days (fig. S2A, B; thus, the whole collection of the dsRNAs was screened 4 times). After dsRNA treatment, $[Ca^{2+}]_{mito}$ and $[H^+]_{mito}$ were measured in each well before and after addition of thapsigargin. Our screen achieved high signal-to-noise ratios and low well-to-well variation (fig. S3C). The scatter plot for values from duplicate wells demonstrates the reproducibility of the screen (fig. S3D).

From the primary screen, we identified a total of 776 hits according to the calculated Z-score (Table S1). Each hit was assigned a score according to their inhibition of $[Ca^{2+}]_{mito}$ and/or $[H^+]_{mito}$ changes relative to positive controls (*olf186-F* - CRAC channel, *Thread* - *Drosophila* inhibitor of apoptosis, and *Rho1* - *Ras*-like small GTPase). The majority of these genes were essential for cell viability (ribosomal proteins, mitotic proteins, transcription factors, etc; fig. S3E), and are commonly identified in other genome-wide screens. Reassuringly, all genes previously shown to regulate cytoplasmic Ca^{2+} (*SERCA*, *PMCAs*, *Stim1*, and the *CRAC/Orai* homolog, *olf186-F*) were among the most statistically significant hits. Of the genes encoding known mitochondrial proteins, many had well-defined functions (e.g., TOMM/TIMM complex proteins, respiratory chain subunits, metabolic enzymes). Genes encoding proteins of less well-characterized function, as well as some positive and negative controls, were tested in a secondary screen (Table S2). The influence of candidate genes on mitochondrial Ca^{2+} and H^+ transport were then characterized in detail. dsRNAs against *Drosophila UCP* homologs did not affect $[Ca^{2+}]_{mito}$ and $[H^+]_{mito}$ changes induced by thapsigargin in intact cells or by Ca^{2+} applied to permeabilized S2 cells (fig. S4).

After the secondary screen, false-positive and relatively weak hits were eliminated from further consideration. A group of 10 genes were identified as potential candidates for mitochondrial Ca^{2+} transporters (Table S3). Comprehensive bioinformatic analyses eliminated genes containing no putative transmembrane spanning segments or lacking human orthologs. *CG4589*, the *Drosophila* homolog of a human gene named *Letm1* (*dLetm1*), was the sole hit satisfying all criteria and was the gene with the strongest impact on $[Ca^{2+}]_{mito}$ and $[H^+]_{mito}$ responses.

Discussion
At high $[Ca^{2+}]_{cyto}$, MCU/MiCa is a rapid, high capacity Ca^{2+} influx mechanism. It rapidly depolarizes mitochondria, but it cannot restore $Ca^{2+}{}_{mito}$ as MiCa's outward conductance is negligible under physiological conditions(*2*). We did not identify the gene encoding the

MCU/MiCa channel in our genome-wide screen, probably due to functional redundancy of multiple Ca^{2+} transporters, and future studies will be required to identify this gene.

Based on the result that the valinomycin dependent, K^+ diffusion membrane potential accelerated the Ca^{2+} transport rate in liposomes, we hypothesize that the Letm1 activity depends on transmembrane voltage. Experiments under voltage control will be required to refine the estimated stoichiometry and to understand how this may affect the actions of Letm1 in cells.

The mitochondrial alkalinization observed in some experiments may result, in part, from Ca^{2+} activation of mitochondrial metabolic enzymes. Ca^{2+} may, however, directly or indirectly stimulate F_0F_1ATPase activity, increasing the overall ATP production rate and resulting in more H^+ influx. Ca^{2+} may also directly stimulate metabolite carriers, some of which also cause H^+ influx. Thus, the net pH change caused by the effect of Ca^{2+} on oxidative phosphorylation requires a detailed comparison of all proton pathways.

In mitochondria, Ca^{2+} and H^+ are critical regulators of mitochondria's primary function of oxidative phosphorylation. Mitochondria are well known to have significant Ca^{2+} buffering and storage capacity, but if Ca^{2+} influx is not compensated by efflux, apoptosis of the cell ensues. The Letm1 Ca^{2+}/H^+ exchanger mechanism is a critical component for mitochondrial $[Ca^{2+}]$ and $[H^+]$ homeostasis.

Materials and Methods

1. Generation of pericam stable cell lines

Drosophila S2 cells were transfected with pericam sub cloned into the PMK33 vector (gene expression controlled by a *Drosophila* metallothionein promoter). Pericam expressing S2 cells were selected by applying 400 μM hygromycin. A stable, tetracycline inducible Flp-In-293-pericam cell line was generated according to the manufacturer's instructions.

2. Genome-wide *Drosophila* RNAi screen

The high-throughput *Drosophila* RNAi screen was conducted according to protocols as previously described(*14*) with slight modifications. Briefly, $2.5X10^4$ S2-pericam cells were dispensed to each well of 384-well plates containing 0.25 μg dsRNA in 10 μl of Schneider's medium without serum (Invitrogen). After 60 min of incubation with dsRNAs, cells were supplemented with 30 μl of *Drosophila* SFM (Invitrogen) with 0.75 μM $CuSO_4$ and incubated at 24^oC for 3 or 5 days. Before fluorescence measurements, the cell media were changed to Krebs-Ringer-HEPES (KRH) buffer (125 mM NaCl, 5 mM KCl, 1.2 mM KH_2PO_4, 6 mM glucose, 1.2 mM $MgCl_2$, 2 mM $CaCl_2$, and 25 mM HEPES, pH 7.4). Fluorescence measurements were performed before and after the application of 1 μM thapsigargin using an Analyst GT plate reader (Molecular Devices). Original fluorescence readings from 430 and 490 nm excitation were collected and converted to F_{490}/F_{430}, $-\Delta F_{430}/F_0$, or $-\Delta F_{490}/F_0$. A Z-score was calculated for each well ($[F_{well}-F_{plate\text{-}mean}]/SD_{plate}$). Hits were selected using bar graph based analyses as well as the Heatmap tool from the *Drosophila* RNAi Screening Center (http://flyrnai.org/cgi-bin/RNAi_heatmap_public.pl). Commonly identified hits in other genome-wide screens can be searched from the database (http://flyrnai.org/cgi-bin/RNAi_gene_lookup_public.pl). Alternatively designed dsRNAs were tested for nearly half of the genes in the secondary screen.

3. Mammalian cell transfection

HeLa and Flp-In-293 cells were transfected with Effectene (Qiagen) according to the manufacturer's instructions. Full-length cDNA of human *Letm1* (BC021208) was obtained from Open Biosystems and subcloned in frame with a C-terminal sequence encoding the Cherry fluorescence protein.

4. RNAi in *Drosophila* and mammalian cells

dsRNAs against *Drosophila* were synthesized with the MEGAscript in vitro transcription kit (Ambion) using PCR fragments of the corresponding cDNAs as templates. siRNAs against human *Letm1* and standard scrambled control siRNAs were purchased from Ambion. HeLa cells were transfected with siRNAs using Lipofectamine RNAiMAX (Invitrogen) and incubated for 3 days before experiments. Concentrations of *olf186-F* dsRNAs were 10-100 times lower than the standard concentration used in the screen in order to optimize the experimental protocol for achieving efficient and consistent RNAi (data not shown). Sense sequence for *Letm1*-siRNA#1: UCCACAUUUGAGACUCAGUtt, *Letm1*-siRNA#2: AUGUUCCAUUUGGCUGCUGtt.

5. $[Ca^{2+}]_{mito}$, $[H^+]_{mito}$, $[Ca^{2+}]_{cyto}$, and Ψ_{mito} measurements

Fluorescence measurements of cells expressing pericam were made using a FluoView 1000 confocal microscope (Olympus) in KRH buffer (intact cells). For experiments with permeabilized cells, 100 μM digitonin was briefly applied followed by 10 min perfusion in intracellular solution (120 mM KCl, 0.5 mM KH_2PO_4, 10 mM succinate, 10 mM HEPES) with 1 mM EGTA. The cells were constantly perfused with intracellular medium with $[Ca^{2+}]$ as indicated. $[Ca^{2+}]_{mito}$ and $[H^+]_{mito}$ were monitored at 405 nm and 488 nm excitation, respectively, and emission was collected at ~ 530 nm. The pH dependent $[Ca^{2+}]_{mito}$ and $[H^+]_{mito}$ experiments were performed using solutions containing BAPTA at the concentrations indicated. $[Ca^{2+}]_{cyto}$ was measured by loading the cells with 10 μM Fluo-4 AM (Molecular Probes), measured at 488 nm excitation and 530 nm emission. Ψ_{mito} was measured using TMRM (Molecular Probes). Cells were loaded with 5 nM TMRM for 10 min, and the fluorescence levels (at 580 nm) measured from 543 nm excitation. Sharp cutoff dichroic emission filters enabled precise control of the excitation and emission wavelengths.

6. Isolation of Mitoplasts

Mitochondria were isolated by differential centrifugation as previously described(*2*). Isolated mitochondria were stored on ice in solution with 250 mM sucrose, 5 mM HEPES, and 1 mM EGTA (pH 7.2 with KOH). To remove the outer membrane, mitochondria were subjected to osmotic shock for 10 min in hypotonic solution containing 5 mM sucrose, 5 mM HEPES, and 1 mM EGTA (pH 7.2 with KOH) and resuspended in intracellular solution.

7. Ca^{2+}_{mito} uptake into artificial liposomes by purified Letm1

Letm1-His bacterial expression and His-tag purification was conducted as previously described(*15*) with slight modifications. Isolated Letm1-His proteins (50 μg/ml) were diluted to a final concentration of 2 μg/ml for liposome reconstitution. 100 mg/ml asolectin and 10 mg/ml cardiolipin were sonicated until clear and mixed with 2 μg/ml purified Letm1 protein, 1.4% TritonX-114. Detergent was removed by passing the mixture multiple times through Amberlite XAD-2 columns. Extraliposomal solutions were changed by passing through PD-10 desalting columns X2. Letm1 proteoliposome size was 374 ± 185 nm (Zetasizer Nano ZS, Malvern Instruments). $[Ca^{2+}]$ was measured by 10 μM Fluo-4 salt, or Fluo-5N (Invitrogen), and pH measured by 10 μM Snarf-5F (Invitrogen). Free $[Ca^{2+}]$ or pH changes were calculated from initial dye calibration. Total $[Ca^{2+}]$ was calculated using WEBMAXC (http://www.stanford.edu/~cpatton/webmaxcS.htm).

For experiments in Fig. 4B, liposome and external solution contained 200 mM HEPES, 100 mM TMA-OH, 1 mM BAPTA (free acid), pH 7.4; Ca^{2+} was added to create an initial free $[Ca^{2+}]$ = 750 nM. Changes in free $[Ca^{2+}]$ were measured by the Ca^{2+}-sensitive fluorescent dye Fluo-4; total $[Ca^{2+}]$ was calculated using WEBMAXC.

For Fig. 4C, liposomes were loaded with 240 mM HEPES, 60 mM TMA-OH, 1 μM $CaCl_2$ at pH 7.0. Solution contained 0.5 mM HEPES-TMA, 300 mM sucrose, 1 μM

$CaCl_2$, with initial pH = 7.0. Changes in pH were measured by the pH-sensitive fluorescent dye Snarf-5F.

For Fig. 4D,E, Liposomes were loaded with 230 mM HEPES, 70 mM TMA-OH, 1 μM $CaCl_2$ at pH 7.2. Solution contained 1 mM HEPES-TMA, 300 mM sucrose, 1 μM $CaCl_2$, pH 7.2. HEPES-MES (50 mM, pH 6.5) or HEPES-Tris (50 mM, pH 8.0) was added as indicated. Changes in [Ca^{2+}] were measured by Fluo-5N.

For Fig.4F, total Ca^{2+} added was increased while free [Ca^{2+}] remained < 1 μM by adjusting the concentration of Ca^{2+} chelator. Calcium (/μg protein; 70, 210, 700, 2100 nmol) was added in buffers containing BAPTA (0.1, 0.3, 1, 3 mM) to an initial free [Ca^{2+}] = 750 nM.

References

S1. R. Rizzuto, P. Bernardi, T. Pozzan, *J Physiol* **529 Pt 1**, 37 (Nov 15, 2000).
S2. Y. Kirichok, G. Krapivinsky, D. E. Clapham, *Nature* **427**, 360 (Jan 22, 2004).
S3. G. Szabadkai, M. R. Duchen, *Physiology (Bethesda)* **23**, 84 (Apr, 2008).
S4. G. Hajnoczky, L. D. Robb-Gaspers, M. B. Seitz, A. P. Thomas, *Cell* **82**, 415 (Aug 11, 1995).
S5. K. K. Gunter, T. E. Gunter, *J Bioenerg Biomembr* **26**, 471 (Oct, 1994).
S6. P. Bernardi, *Physiol Rev* **79**, 1127 (Oct, 1999).
S7. N. Demaurex, D. Poburko, M. Frieden, *Biochim Biophys Acta* **6**, 6 (Jan 6, 2009).
S8. D. G. Nicholls, *Biochim Biophys Acta* **1777**, 550 (Jul-Aug, 2008).
S9. A. Rasola, P. Bernardi, *Apoptosis* **12**, 815 (May, 2007).
S10. M. Giacomello, I. Drago, P. Pizzo, T. Pozzan, *Cell Death Differ* **14**, 1267 (Jul, 2007).
S11. T. Nagai, A. Sawano, E. S. Park, A. Miyawaki, *Proc Natl Acad Sci U S A* **98**, 3197 (Mar 13, 2001).
S12. S. Feske *et al.*, *Nature* **441**, 179 (May 11, 2006).
S13. S. L. Zhang *et al.*, *Proc Natl Acad Sci U S A* **103**, 9357 (Jun 13, 2006).
S14. N. Ramadan, I. Flockhart, M. Booker, N. Perrimon, B. Mathey-Prevot, *Nat Protoc* **2**, 2245 (2007).
S15. J. A. Mayor *et al.*, *J Bioenerg Biomembr* **29**, 541 (Dec, 1997).

Fig. S1. Pericam-based simultaneous measurement of $[Ca^{2+}]_{mito}$ and $[H^{+}]_{mito}$ in S2 cells. (A) Representative images of an isolated mitochondrion from S2-pericam cells (left). Mitoplast after the outer membrane was disrupted by osmotic shock (right). Note that pericam is located in the mitochondrial matrix. Scale bar = 2 µm. **(B)** Representative traces of $[Ca^{2+}]_{mito}$ and $[H^{+}]_{mito}$ measured from 405 nm and 488 nm excitation, respectively. Cells were permeabilized briefly with 100 µM digitonin, washed with digitonin-free intracellular solution for 10-15 min, and placed in various $[Ca^{2+}]$ (n=3, 104 cells) or pH (n=3, 123 cells) as indicated, in the presence of 10 µM ionomycin (or 4-Bromo-A23187) and 20 µM FCCP. Ionomycin (or 4-Bromo-A23187) Ca^{2+} ionophores, and FCCP protonophore, dissipate the mitochondrial membrane potential and allow Ca^{2+} and H^{+} to move along their respective concentration gradients. **(C)** $[Ca^{2+}]_{mito}$ and $[H^{+}]_{mito}$ measured as in **B**. F_0 is the pericam fluorescence level in intact S2 cells in normal KRH buffer. Cells were then permeabilized briefly, washed, and placed in various $[Ca^{2+}]$ (n=3, 86 cells) or pH (n=3, 102 cells) as indicated, in the presence of 10 µM 4-Bromo-A23187 and 20 µM FCCP. Data shown are mean ± S.E.M.

Fig. S2. Simultaneous measurement of $[Ca^{2+}]_{mito}$ and $[H^{+}]_{mito}$ in intact S2 cells. (A) Representative traces of $[Ca^{2+}]_{mito}$ and $[H^{+}]_{mito}$ signals in response to FCCP in S2-pericam cells (n=3 , 132 cells). **(B)** Representative traces of thapsigargin-induced changes in $[Ca^{2+}]_{mito}$ and $[H^{+}]_{mito}$ in S2-pericam cells (n=3, 117 cells).

Fig. S3. Genome-wide *Drosophila* RNAi screen for mitochondrial Ca^{2+} transporters. *Drosophila* S2 cells stably expressing mitochondrial-targeted ratiometric pericam were incubated with arrayed double-stranded (ds)RNAs against each of the ~22,000 *Drosophila* genes. Two independent screens were performed with RNAi incubation for either 3 or 5 days. The highly Ca^{2+}-selective *Drosophila* Orai/CRAC channel (*olf186-F*) served as a positive control. **(A)** Schematic diagram of the screening protocol. **(B)** Knockdown of CRAC (olf186-F) inhibited changes in mitochondrial $[Ca^{2+}]$ and $[H^{+}]$ upon 1 µM thapsigargin stimulation. Mitochondrial Ca^{2+} and H^{+} levels in *Drosophila* S2 cells were measured at 405 nm and 488 nm excitation wavelengths of stably transfected pericam. Ionomycin (5 µM) was applied to elicit maximum Ca^{2+} entry. Data shown are representative traces from cells treated with scrambled control (black line; n=3, 94 cells) or *olf186-F* dsRNAs (red or blue line; n=3, 87 cells). **(C)** Heatmap view of a representative 384-well screen plate with dsRNAs against *olf186-F* (CRAC channel; 13A and 14P), *Thread* (DIAP1; 13B, 13G, 14O and 14J) and *Rho1* (13D, 13E, 14N and 14K) as positive controls and dsRNAs against GFP (13C, 13F, 14M and 14L) as negative controls. Values are Z-scores ($[F_{well}-F_{plate\text{-}mean}]/SD_{plate}$) derived from $-\Delta F_{430}/F_0$ of each well. **(D)** Scatter plot for the Z-scores of thapsigargin-induced $[Ca^{2+}]_{mito}$ changes from duplicate screen wells (from the 5-day RNAi screen, 3 min after thapsigargin application). **(E)** Functional classification of the hits from the primary screen. 'Housekeeping' genes encode ribosomal, proteasomal, cytoskeletal, chromosomal, Golgi, TOMM/TIMM complex, respiratory chain subunits, and metabolic enzyme proteins.

Fig. S4. UCP2, 3 homolog knockdown does not affect changes in $[Ca^{2+}]_{mito}$ and $[H^{+}]_{mito}$. (A) Thapsigargin induced $[Ca^{2+}]_{mito}$ and $[H^{+}]_{mito}$ changes in S2-pericam cells treated with a mixture of dsRNAs against *UCP4* and *5* (labeled 'UCP'; squares; n=3, 97 cells), the *Drosophila UCP* homologues of *UCP2* and *UCP3*. **(B)** $[Ca^{2+}]_{mito}$ and $[H^+]_{mito}$ measurements in digitonin-permeabilized S2-pericam cells treated with dsRNAs against *UCP4* and *5* (squares; n=3, 72 cells). Ca^{2+} was applied as indicated. Short-dashed lines indicate control levels. Data shown are mean values ± S.E.M.

Fig. S5. Calibration of basal $[Ca^{2+}]_{mito}$ and $[H^+]_{mito}$ in control and dLetm1 knockdown cells. S2-pericam cells treated with scrambled control (n=3, 117 cells) or *dLetm1* dsRNA (n=3, 96 cells) were permeabilized briefly, washed, baseline fluorescence measured (at 405 nm and 488 nm excitation), and the cells placed in various $[Ca^{2+}]$ or pH as indicated, in the presence of 10 µM ionomycin and 20 µM FCCP. F_0 is the fluorescence level in 1mM EGTA solution (405 nm) and pH 7.0 (488 nm). Data shown are mean ± S.E.M.

Fig. S6. HeLa $[Ca^{2+}]_{mito}$ and $[H^+]_{mito}$ in 10 and 2 mM $[Ca^{2+}]_o$. (A) mt-pericam is targeted to mitochondria in HeLa cells. **(B)** High external $[Ca^{2+}]$ prolongs histamine-induced $[Ca^{2+}]_{cyto}$ changes in HeLa cells (10 mM $[Ca^{2+}]_o$: red lines; n=3, 91 cells) compared to lower Ca^{2+} (2 mM $[Ca^{2+}]_o$: black lines; n=3 , 87 cells). **(C)** Representative traces of histamine-induced changes in $[Ca^{2+}]_{mito}$ and $[H^+]_{mito}$ in 2 mM $[Ca^{2+}]_o$ (black lines, n=5, 98 cells) or 10 mM $[Ca^{2+}]_o$ (colored lines; n=3, 52 cells). High and low $[Ca^{2+}]_o$ resulted in indistinguishable $[Ca^{2+}]_{mito}$. High $[Ca^{2+}]_o$ was not correlated with the late H^+ influx observed in lower $[Ca^{2+}]_o$.

Fig. S7. Letm1 knockdown increases basal Ψ_{mito} in HeLa cells. (A) Representative images of HeLa cells treated with scrambled control (left) or *Letm1* siRNA (right) and loaded with 5 nM TMRM for 10 min. **(B)** TMRM fluorescence level in scrambled control (left; n = 3, 53 cells) or *Letm1* siRNA-treated (right; n=3, 67 cells) HeLa cells. Data shown are mean ± S.E.M. The asterisks indicate P<0.05 in a two-tailed Student's *t* test.

Fig. S8. Ca^{2+} uptake in Letm1 proteoliposomes. (A) Ca^{2+} addition initially increased external $[Ca^{2+}]$ (measured with Fluo-4), followed by Ca^{2+} import as indicated by falling fluorescence (triangles; n=3). Ca^{2+} uptake was blocked by RuR (10 nmol/µg, circles; n=3), which was reversed by the Ca^{2+} ionophore, 4-Bromo-A23187 (5 µM). Ruthenium 360 similarly inhibited Ca^{2+} uptake (not shown). Ca^{2+} uptake by Letm1 proteoliposomes loaded with 200 mM HEPES, 3 mM BAPTA, 80 mM KCl, pH 7.4 (NaOH), without (triangles; n=3) and with (circles; n=3) 10 nmol/µg Ruthenium Red. Valinomycin (50 nM) was added at time 0 to generate a K^+ diffusion membrane potential. **(B)** Calculated Ca^{2+} transport velocity (nmol/µg protein/s) was plotted against various transliposomal K^+ gradients. Experiments were done as in **A** but with 0, 20, 50 mM KCl added to the external solution to obtain the different K^+ gradients (n=3). Ca^{2+} transport velocity in 0 K^+ gradient was measured in liposomes loaded in K^+-free buffer. All data shown are mean ± S.E.M. The asterisk indicates P<0.05 in a two-tailed Student's *t* test.

Fig. S9. Letm1 structural prediction. Structural prediction of human full-length Letm1 sequence by *Robetta* (http://robetta.bakerlab.org/), displayed using PyMOL. The Letm1-like domain is evolutionarily conserved in Letm1 isoforms and homologous genes. The long α-helices domain shown below is assumed to extend into the mitochondrial matrix.

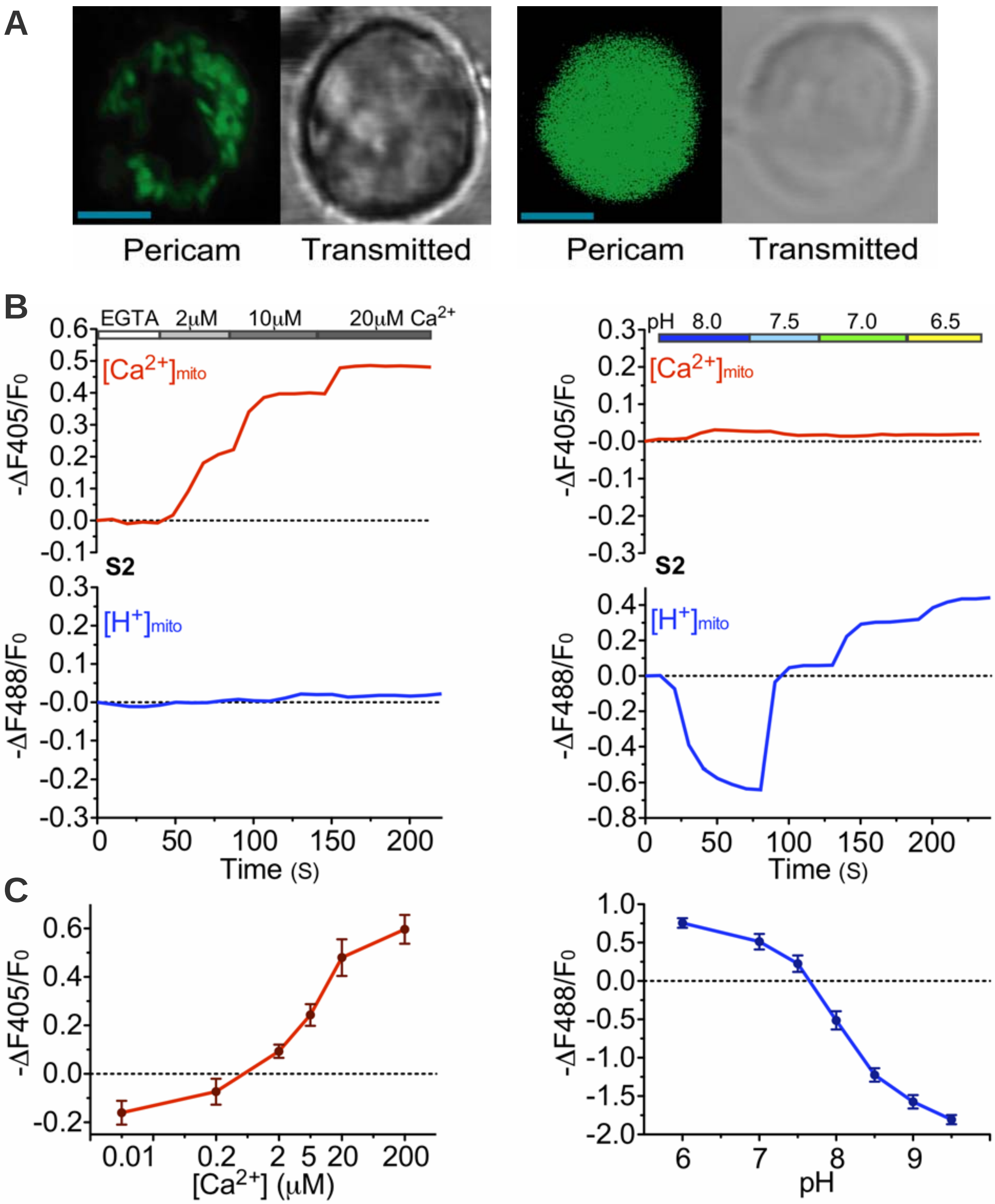

A
Pericam
Transmitted
Pericam
Transmitted
B
EGTA 2μM 10μM 20μM Ca2+
[Ca2+]mito
-ΔF405/F0
S2
[H+]mito
-ΔF488/F0
Time (S)
pH 8.0 7.5 7.0 6.5
[Ca2+]mito
-ΔF405/F0
S2
[H+]mito
-ΔF488/F0
Time (S)
C
-ΔF405/F0
[Ca2+] (μM)
-ΔF488/F0
pH

Figure S1

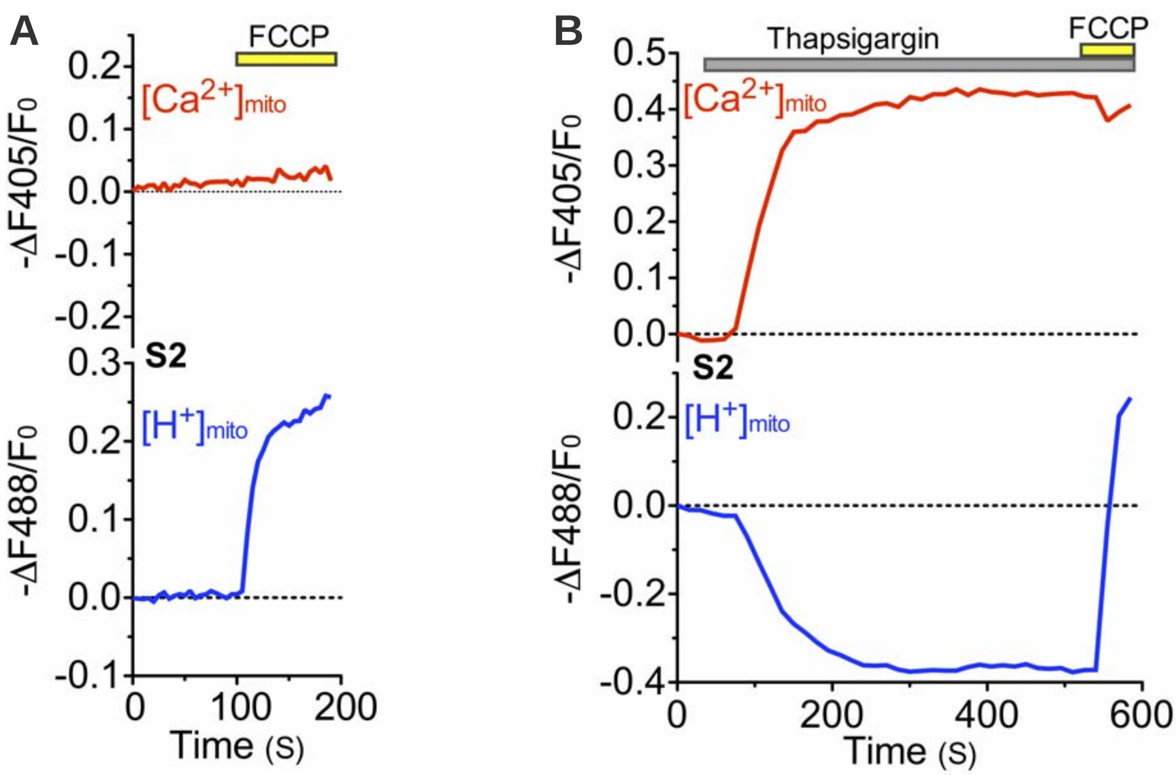
A
FCCP
[Ca2+]mito
-ΔF405/F0
0.2
0.1
0.0
-0.1
-0.2
S2
0.3
[H+]mito
-ΔF488/F0
0.2
0.1
0.0
-0.1
0
100
200
Time (S)
B
Thapsigargin
FCCP
0.5
0.4
0.3
0.2
0.1
0.0
[Ca2+]mito
-ΔF405/F0
S2
[H+]mito
-ΔF488/F0
0.2
0.0
-0.2
-0.4
0
200
400
600
Time (S)

Figure S2

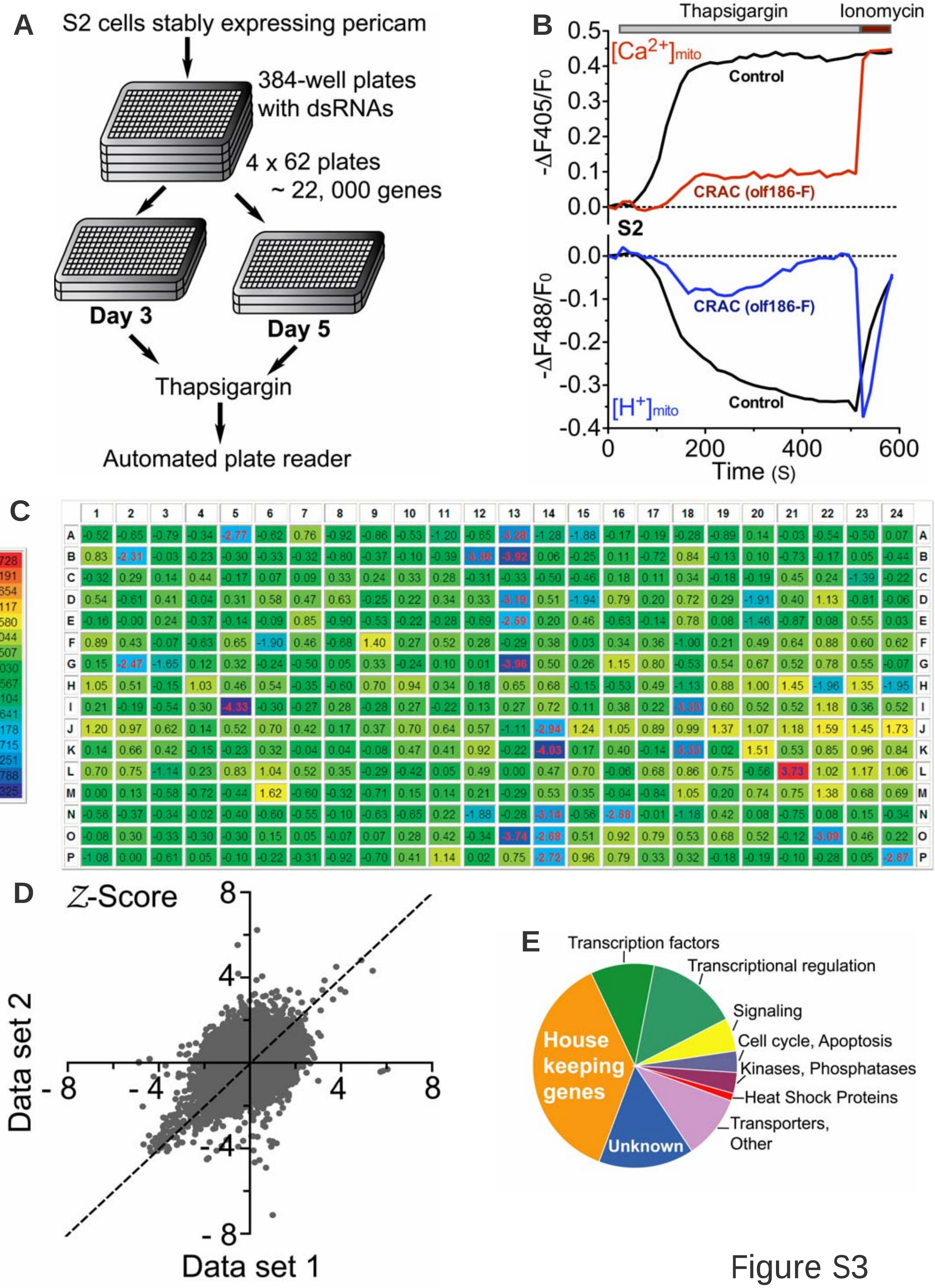

A
S2 cells stably expressing pericam
384-well plates with dsRNAs
4 x 62 plates ~ 22, 000 genes
Day 3
Day 5
Thapsigargin
Automated plate reader
B
Thapsigargin
Ionomycin
[Ca2+]mito
Control
CRAC (olf186-F)
-ΔF405/F0
S2
-ΔF488/F0
[H+]mito
Time (S)
C
D
Z-Score
Data set 1
Data set 2
E
Transcription factors
Transcriptional regulation
Signaling
Cell cycle, Apoptosis
Kinases, Phosphatases
Heat Shock Proteins
Transporters, Other
House keeping genes
Unknown

Figure S3

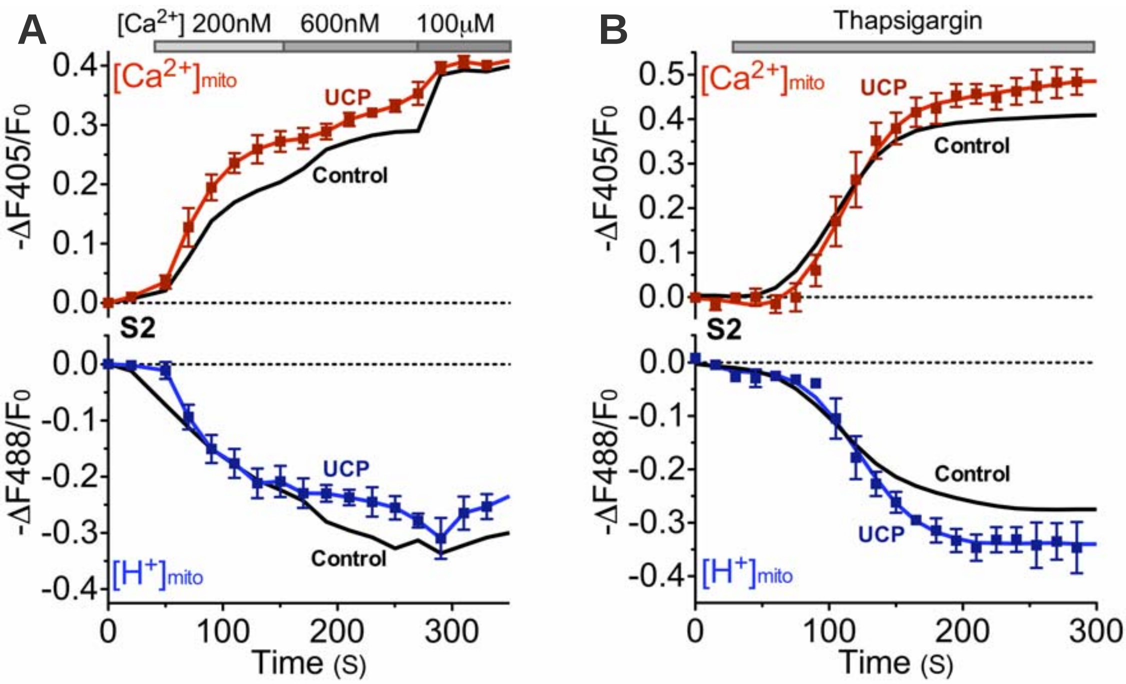

A
[Ca2+] 200nM
600nM
100μM
[Ca2+]mito
UCP
Control
-ΔF405/F0
S2
-ΔF488/F0
UCP
Control
[H+]mito
Time (S)
B
Thapsigargin
[Ca2+]mito
UCP
Control
-ΔF405/F0
S2
-ΔF488/F0
Control
UCP
[H+]mito
Time (S)

Figure S4

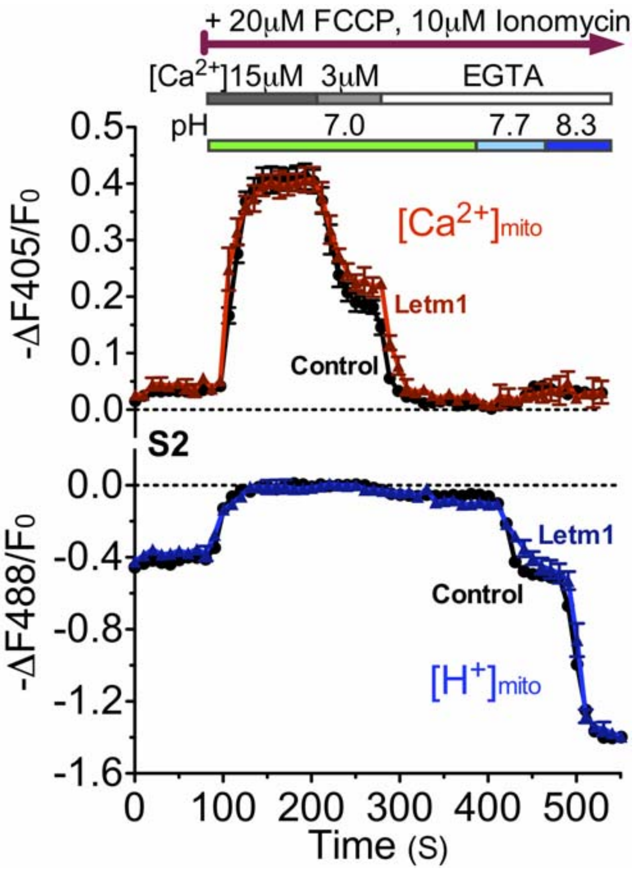
+ 20μM FCCP, 10μM Ionomycin
[Ca2+] 15μM 3μM EGTA
pH 7.0 7.7 8.3
[Ca2+]mito
Letm1
Control
-ΔF405/F0
S2
Letm1
Control
[H+]mito
-ΔF488/F0
Time (S)

Figure S5

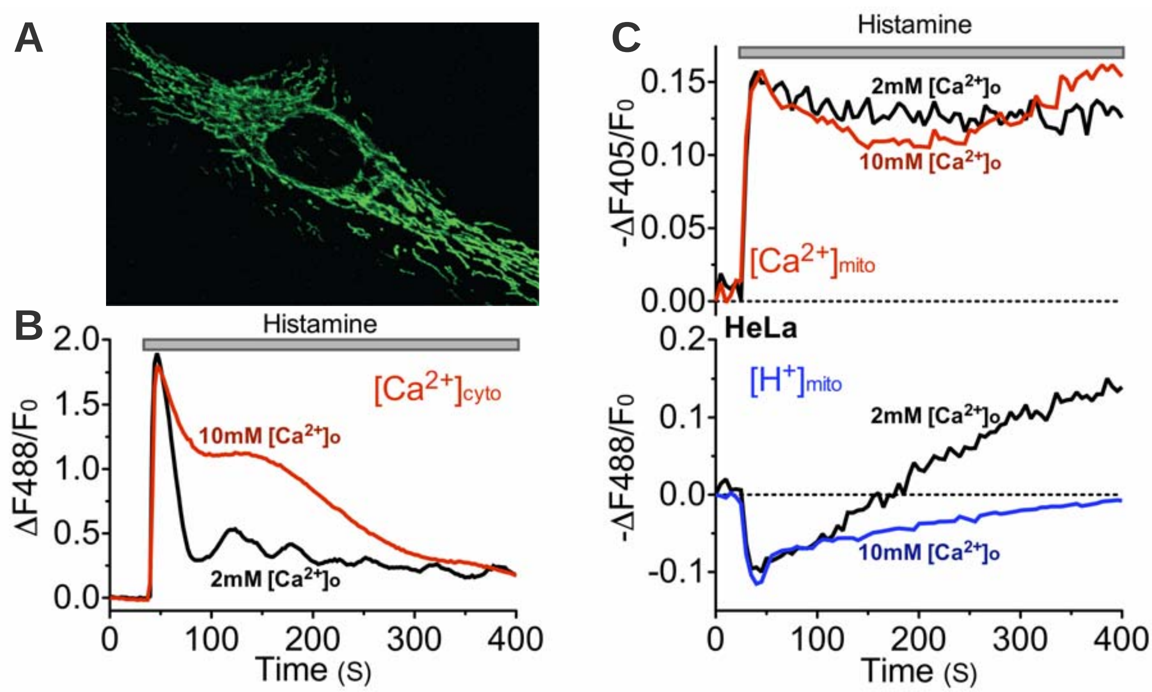
A
B
Histamine
[Ca2+]cyto
10mM [Ca2+]o
2mM [Ca2+]o
ΔF488/F0
Time (S)
C
Histamine
2mM [Ca2+]o
10mM [Ca2+]o
[Ca2+]mito
-ΔF405/F0
HeLa
[H+]mito
2mM [Ca2+]o
10mM [Ca2+]o
-ΔF488/F0
Time (S)

Figure S6

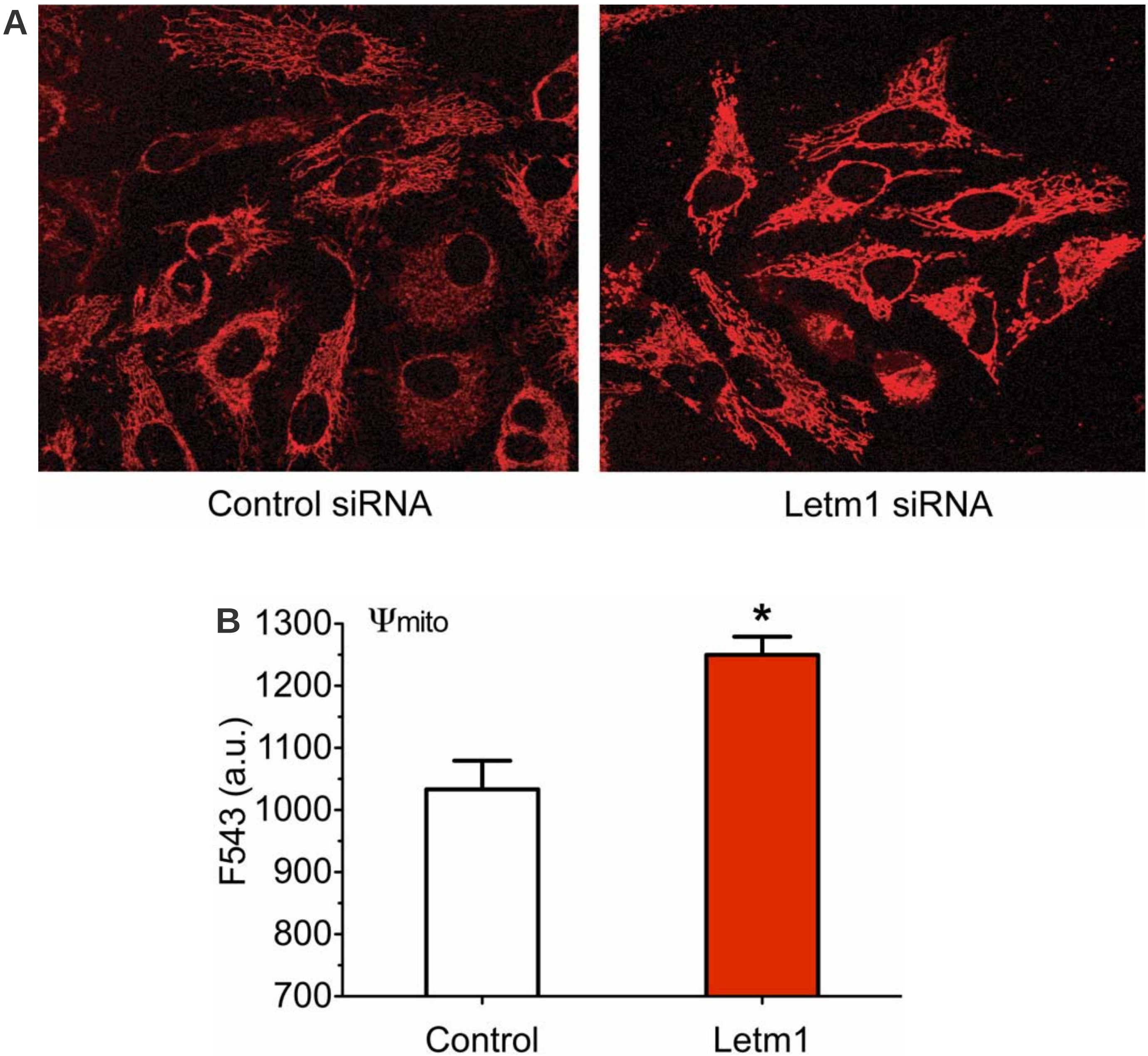
A
Control siRNA
Letm1 siRNA
B
Ψmito
*
1300
1200
1100
1000
900
800
700
F543 (a.u.)
Control
Letm1

Figure S7

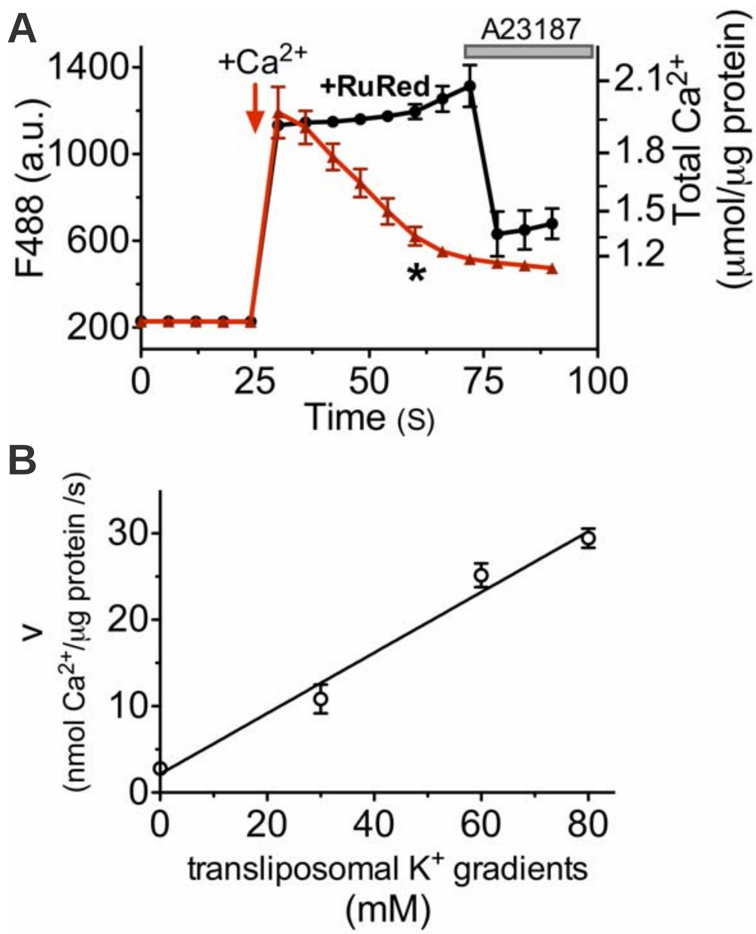
A
B
+Ca2+
+RuRed
A23187
F488 (a.u.)
Total Ca2+ (μmol/μg protein)
Time (S)
v (nmol Ca2+/μg protein /s)
transliposomal K+ gradients (mM)

Figure S8

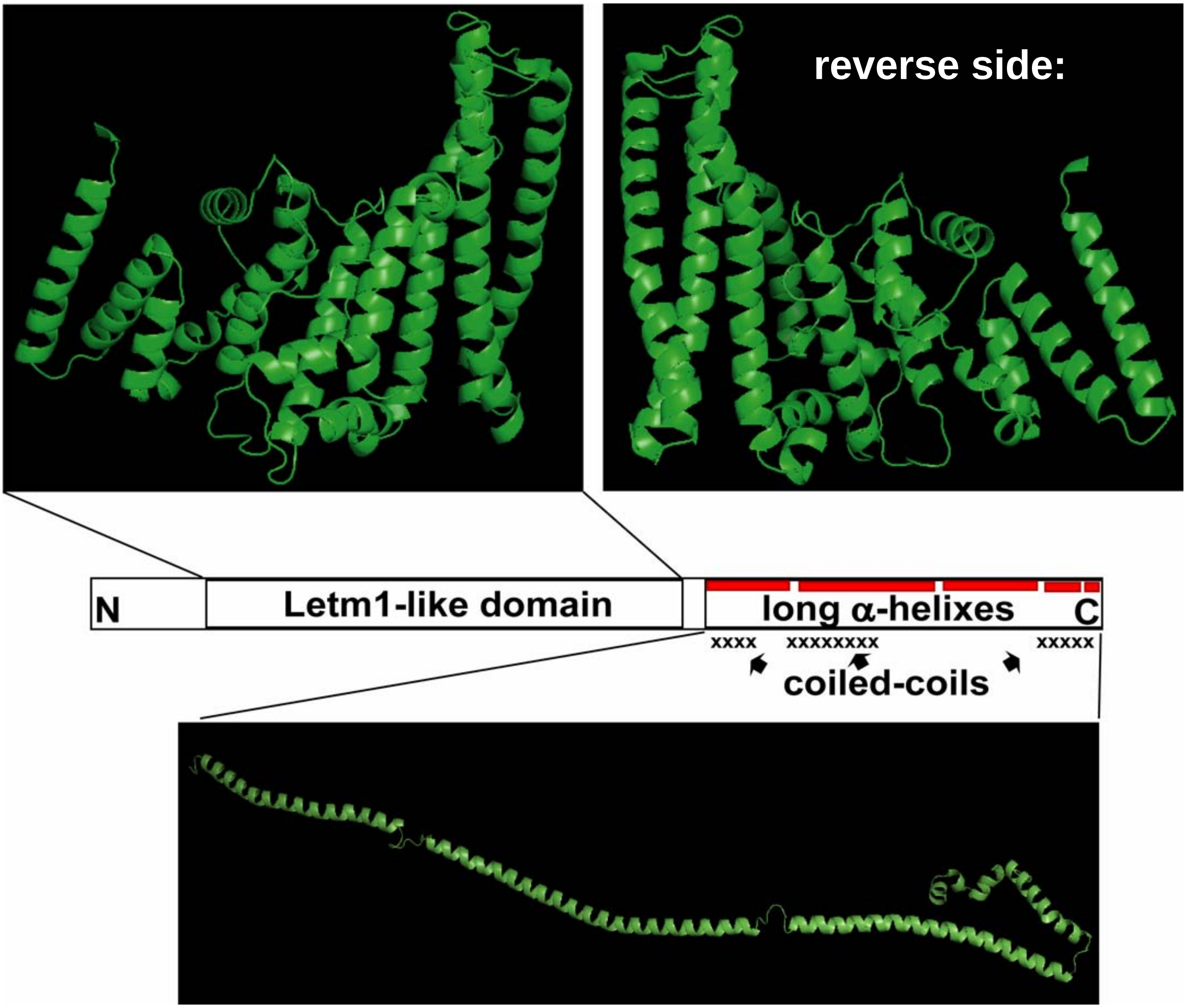
reverse side:
N
Letm1-like domain
long α-helixes
C
xxxx
xxxxxxxx
xxxxx
coiled-coils

Figure S9

Table S1. Hits from the primary screen.

Each gene identified from the primary screen was assigned a score based on relative $[Ca^{2+}]_{mito}$ and $[H^{+}]_{mito}$ changes compared to positive controls (olf186-F, Thread and Rho1). Genes with similar inhibitory effects as the positive controls were assigned a score of 3; those showing 50-75% inhibition compared to control levels were scored as 2, and 25-50% of control levels as 1. Off-target effects of each amplicon were predicted by DRSC based on exact 21 nucleotide homology searches.

DRSC Amplicon	Of Interest	Gene	Human Homologene	19 bp Matches
DRSC23852	1	phol		0
DRSC25951	1	Rpn7	PSMD6	0
DRSC25879	1	sta	RPSA	0
DRSC25776	3	MED25		0
DRSC25781	1	Smr		0
DRSC23542	2	Spx	SF3B4	0
DRSC23432	1	MED31	MED31	0
DRSC25109	1	Rm62		0
DRSC25032	1	RpL4	RPL4	0
DRSC23411	1	RpLP1	RPLP1	0
DRSC25850	2	CG33859	HIST2H2AB	24
DRSC23587	1	MED14	CRSP2	0
DRSC25135	1	MED4	MED4	0
DRSC26355	2	RpS30	FAU	0
DRSC26152	2	noi	SF3A3	0
DRSC26269	3	Tbp-1	PSMC3	0
DRSC26498	3	CG3523	FASN	0
DRSC26497	2	Su(Tpl)	ELL2	0
DRSC26633	1	MED16	THRAP5	0
DRSC26650	3	beta'Cop	COPB2	0
DRSC26462	2	CG13298	SF3B14	0
DRSC26839	2	CG14641	RBM22	0
DRSC26931	1	zfh1	ZEB1	0
DRSC27065	1	CG1109	WDR33	0
DRSC26760	2	sop	RPS2	0
DRSC27111	2	Rpb11	POLR2J	0
DRSC27157	3	RpII215	POLR2A	0
DRSC28179	2	Klp61F	KIF11	0
DRSC21247	1	Hsp70Bb	Hsp70Bb	7
DRSC01103	1	CG5853		1
DRSC21249	1	LysD	LYZ	3
DRSC05782	1	CG33453		2
DRSC05070	1	CG30379		0
DRSC05621	1	CG30463		9
DRSC03948	1	Dnr1	MYLIP	0
DRSC25542	1	CG14934		0
DRSC24497	1	CG17751		0
DRSC26265	1	CG17752		0
DRSC28203	1	CG9772	SKP2	0

DRSC28078	3	Pros25	PSMA2	0
DRSC28391	1	RpL19	RPL19	0
DRSC28279	2	Rpn5	PSMD12	0
DRSC28558	1	RpS13	RPS13	0
DRSC28234	1	oho23B	RPS21	0
DRSC28394	2	Pp2A-29B	PPP2R1A	0
DRSC28510	1	RpLP2	RPLP2	0
DRSC28578	1	CG14636		0
DRSC28589	2	Rpn12	PSMD8	0
DRSC29446	3	Dox-A2	PSMD3	0
DRSC29788	1	Snap	NAPA	0
DRSC29742	2	TfIIFbeta	GTF2F2	0
DRSC30006	1	CG15609	EHBP1	0
DRSC00708	2	lilli		0
DRSC00268	1	CG3523	FASN	5
DRSC03342	2	Hel25E	BAT1	1
DRSC03492	2	beta'Cop	COPB2	1
DRSC03207	1	CG31673		0
DRSC04697	1	l(2)dtl		1
DRSC07542	3	Rpt1	PSMC2	0
DRSC07324	1	CG9027		0
DRSC07129	1	CG8257	CARS2	0
DRSC07552	1	Sin3A	SIN3A	0
DRSC06854	2	NAT1	EIF4G2	1
DRSC07246	2	lig	UBAP2	223
DRSC07447	2	Jra	JUND	0
DRSC26038	1	CG2843	CCDC49	0
DRSC26580	1	CG7990		0
DRSC26616	1	p130CAS	BCAR1	0
DRSC26626	1	Fak56D	PTK2	0
DRSC26726	1	CG11926	MON1A	0
DRSC26676	1	CG4196	TMEM165	0
DRSC27057	1	CG30087	KLK6	0
DRSC07059	2	CG8046		0
DRSC07293	2	prp8	PRPF8	0
DRSC07159	2	l(2)05070	PSMB6	0
DRSC08235	1	MED14	CRSP2	6
DRSC06023	1	CG11007	TXNDC14	0
DRSC11122	1	CrebA		0
DRSC12186	3	Prosbeta4	PSMB4	0
DRSC11285	1	Snap	NAPA	1
DRSC11775	1	CG5282		0
DRSC12227	2	CG14641	RBM22	1
DRSC09988	1	CG13380		0
DRSC11404	3	th		0
DRSC10954	3	Su(Tpl)	ELL2	1
DRSC16107	1	CG6752	RNF123	0
DRSC16831	2	RpII140	POLR2B	0
DRSC16133	2	Fer3		2

DRSC15166	2	CG16941	SF3A1	0
DRSC27103	1	bgm	ACSBG2	0
DRSC26876	1	mRpL44	MRPL44	0
DRSC27253	1	CG31523		0
DRSC27135	1	CG5720	ZC3H14	0
DRSC27264	1	mRpL40	MRPL40	0
DRSC27518	1	Ugt35b	UGT2B17	0
DRSC27631	1	CG15525	CCDC12	0
DRSC28007	1	Ntl		0
DRSC28015	1	CG33255, CR32205		8
DRSC28055	1	SNF1A	PRKAA2	0
DRSC28874	1	ine		0
DRSC28927	1	Corin		0
DRSC16223	2	Rrp6	EXOSC10	0
DRSC16801	2	Prosbeta3	PSMB3	0
DRSC16068	2	Rpb7	POLR2G	0
DRSC12608	1	TfIIFalpha	GTF2F1	5
DRSC14594	1	RpI12	ZNRD1	1
DRSC16799	3	Pros26.4	PSMC1	2
DRSC16810	2	Rab7	RAB7A	0
DRSC15948	1	CG6015	CDC40	0
DRSC16150	2	Nup133	NUP133	0
DRSC16842	1	Tbp-1	PSMC3	1
DRSC16006	1	CG6271		5
DRSC16841	3	Rpn7	PSMD6	1
DRSC18482	1	Suv4-20		7
DRSC18712	1	RpS6	RPS6	4
DRSC17135	2	gw	TNRC6C	0
DRSC16839	3	Rpn2	PSMD1	0
DRSC17148	3	MED26		0
DRSC17743	3	Bx42	SNW1	1
DRSC20158	3	Stim	STIM1	0
DRSC20280	3	RpII215	POLR2A	1
DRSC19450	1	e(y)3		3
DRSC20312	1	betaCop	COPB1	1
DRSC00535	3	CG2807	SF3B1	0
DRSC00713	1	CG8840		0
DRSC03422	2	Rpn11	PSMD14	0
DRSC03356	1	Kr-h2	TMEM33	0
DRSC03546	3	hoip	NHP2L1	0
DRSC03401	2	Pros35	PSMA1	0
DRSC03454	2	TfIIB	GTF2B	0
DRSC02774	2	CG4738	NUP160	0
DRSC28920	1	Ocho		0
DRSC29264	1	Caps	CADPS	0
DRSC29101	1	Dscam	DSCAML1	0
DRSC29097	1	CG5151		0
DRSC29153	1	CG9507		0
DRSC29578	1	sli	SLIT2	0

DRSC29379	1	CG8828		0
DRSC29452	1	CG17264		0
DRSC29640	1	Toll-7		0
DRSC00546	1	Trn-SR	TNPO3	0
DRSC02678	1	CG18585	CPA2	0
DRSC00692	1	mio	FLJ20323	0
DRSC00626	1	CG3662		0
DRSC02639	1	CG17904	NUBP1	0
DRSC03411	1	RfC3	RFC5	0
DRSC03318	3	Dox-A2	PSMD3	0
DRSC03513	1	crc		0
DRSC04644	1	Pros29	PSMA4	0
DRSC04506	2	MED16	THRAP5	2
DRSC04838	2	BubR1		0
DRSC04624	3	Mov34	PSMD7	1
DRSC07501	1	Pabp2	PABPN1	0
DRSC06100	2	Rpb5	POLR2E	0
DRSC08671	3	Klp61F	KIF11	6
DRSC07660	2	par-1	MARK3	0
DRSC08695	3	RpL8	RPL8	1
DRSC08532	3	RpL8	RPL8	1
DRSC07540	2	RpS18	RPS18	0
DRSC08721	3	mge	TOMM22	0
DRSC10944	1	MED24	THRAP4	0
DRSC11182	2	HLH106	SREBF1	0
DRSC12366	3	RpII18	POLR2F	3
DRSC12205	3	MED27	CRSP8	0
DRSC11946	1	CkIIalpha	CSNK2A1	0
DRSC16059	2	MED7	CRSP9	1
DRSC02953	1	CG6412	TSFM	2
DRSC03455	1	TfIIS	TCEA1	4
DRSC02200	1	mRpL51		1
DRSC02161	1	JhI-21	SLC7A5	1
DRSC04699	1	l(2)k09913		0
DRSC06805	1	CG30496	GLMN	0
DRSC04288	1	Eps-15	EPS15L1	0
DRSC04327	1	thoc5	THOC5	0
DRSC04478	1	CG4612		0
DRSC04249	1	CG15658		0
DRSC04722	1	uzip		1
DRSC06803	1	CG1942		0
DRSC07007	1	CG6701		0
DRSC09787	1	CG10724	WDR1	0
DRSC10528	1	thoc6	THOC6	0
DRSC14460	2	CG11985	SF3B5	0
DRSC16832	3	RpII15	POLR2I	0
DRSC15378	2	mor	SMARCC2	1
DRSC16798	2	Pros25	PSMA2	0
DRSC15890	3	CG5844		0

DRSC16955	3	gammaCop		0
DRSC17168	3	RpS3A	RPS3A	0
DRSC14729	1	Slu7	SLU7	1
DRSC18116	3	CG1677	NHN1	0
DRSC18713	3	Rpt4	PSMC6	0
DRSC17794	2	CR11700		3
DRSC20283	3	Rpt3	PSMC4	3
DRSC00708	3	lilli		0
DRSC22061	3	olf186-F	TMEM142A	0
DRSC22819	1	RpL22	RPL22	8
DRSC23203	2	sima		1
DRSC18835	1	snf	SNRPA	0
DRSC20572	1	Rab10	RAB10	2
DRSC20526	2	CG15455	RUNX2	385
DRSC20483	2	CG11566		0
DRSC19555	3	CG14200		736
DRSC20029	1	CG34422	ARID4B	0
DRSC20039	2	CG7349		0
DRSC01084	1	CG31882		0
DRSC20490	1	CG12565		0
DRSC05050	2	CG11166		293
DRSC07746	1	CG40290		3
DRSC07992	1	dos		193
DRSC01577	2	beat-IIIa		0
DRSC05460	1	shot	MACF1	1
DRSC08896	2	Pdp1	HLF	417
DRSC08897	3	Pdp1	HLF	879
DRSC08464	1	CG15011	NFXL1	0
DRSC10540	1	orb2	CPEB4	1
DRSC08204	1	VhaM9.7-1		1
DRSC08591	1	Syx17	STX17	0
DRSC11298	1	Taf2	TAF2	2
DRSC09674	1	CG7207	COL4A3BP	0
DRSC10512	1	PGRP-L	TMEM11	0
DRSC10565	1	CG5989	LETMD1	0
DRSC09772	1	CG10671	C20orf142	1
DRSC08693	1	Rop	STXBP1	2
DRSC11207	1	LanA	LAMA5	0
DRSC12189	1	CG12007	RABGGTA	0
DRSC11800	1	DNApol-eta	POLH	0
DRSC11755	1	CG4365	HAGH	0
DRSC12164	1	Hph	EGLN1	1
DRSC12199	1	CG12170	OXSM	0
DRSC11223	1	Mipp1		0
DRSC13664	2	nAcRalpha-96Aa	CHRNA3	300
DRSC09230	1	CG17672		603
DRSC17126	1	MED26		0
DRSC19214	3	Sh	KCNA2	717
DRSC24702	1	CG11905		0

DRSC24787	2	CG10081		0
DRSC23582	1	Slu7	SLU7	0
DRSC25381	2	Ald		0
DRSC24271	2	CG13213	FBXL6	0
DRSC23615	1	MED15	PCQAP	0
DRSC23497	2	gw	TNRC6C	0
DRSC23458	2	MED19	MED19	0
DRSC23439	2	Fs(2)Ket	KPNB1	0
DRSC25012	2	Pros26.4	PSMC1	0
DRSC23578	3	desat1		0
DRSC25113	1	disco		0
DRSC25532	1	HLHmgamma		0
DRSC23698	1	e(y)3		1
DRSC25108	2	lark	RBM4B	0
DRSC23905	1	Gbp	PRPF19	0
DRSC25105	2	Hsc70-3	HSPA5	0
DRSC24015	1	Hsc70-5	HSPA9	0
DRSC01101	1	CG33300		1
DRSC20576	1	cactin	C19orf29	1
DRSC01236	1	aret	CUGBP2	500
DRSC20678	2	CG12655		0
DRSC01162	2	CG32830		438
DRSC21265	3	CG33870	HIST2H2BF	1
DRSC19487	1	CG12702		1
DRSC20963	2	RpL15		0
DRSC21267	3	CG33818	HIST1H3I	1
DRSC20967	2	CG13865		0
DRSC05553	2	CG30470		210
DRSC07955	2	CG7971	SRRM2	0
DRSC11632	1	Mes2		1
DRSC12583	1	CG31493		0
DRSC15179	1	CG17184	ARFIP2	1
DRSC16968	1	htl	FGFR3	0
DRSC12517	1	CG10277	RNF13	1
DRSC16647	1	Dhod	DHODH	0
DRSC16207	1	CG7156	RPS6KC1	2
DRSC16087	1	CG6660		0
DRSC14393	1	CG11820		0
DRSC16709	1	Hrb98DE	HNRPA1	2
DRSC18393	1	CG5941		0
DRSC18760	1	deltaCOP	ARCN1	1
DRSC18746	1	brn	B3GALT2	0
DRSC16929	1	dco	CSNK1E	1
DRSC19331	1	Anxb11	ANXA7	2
DRSC00746	1	Clp	CPSF4	0
DRSC00813	1	dpp	ARCN1	1
DRSC20625	1	CG14613	C18orf19	2
DRSC13081	2	Su(var)3-9	EIF2S3	0
DRSC13742	1	CG14550		0

DRSC12447	1	Alh	MLLT10	611
DRSC13530	1	CG31353		467
DRSC13637	1	CG31468		0
DRSC08991	3	CG32048		722
DRSC13017	3	foxo	FOXO3	675
DRSC13176	1	bxd		1
DRSC09116	1	CG33272		21
DRSC09263	2	sens		479
DRSC11593	1	Mes2		0
DRSC13670	3	nAcRalpha-96Aa	CHRNA3	103
DRSC17638	2	Hk	KCNAB1	51
DRSC17689	1	CG32808		1
DRSC30091	1	Taf10	TAF10	0
DRSC30085	1	CG32572		0
DRSC25162	1	alphaTub67C		0
DRSC25011	2	alphaTub84B	TUBA1A	1
DRSC24030	2	CG10777	DDX17	0
DRSC23438	3	Cdc27	CDC27	0
DRSC25556	2	c12.1	HSPC148	0
DRSC23424	2	alphaTub85E	TUBA1C	0
DRSC24096	1	CAP-D2	NCAPD2	0
DRSC23516	2	betaTub56D	TUBB2C	4
DRSC23384	2	CR11700		3
DRSC24030	1	CG10777	DDX17	0
DRSC24093	1	CG12309		0
DRSC23475	2	Tango4	PLRG1	0
DRSC24431	2	CG31554		0
DRSC24568	1	CG32233		0
DRSC25542	1	CG14934		0
DRSC24497	1	CG17751		0
DRSC25405	1	CG16884		0
DRSC23464	2	CG34339		0
DRSC25068	3	CG6842	VPS4B	0
DRSC25071	1	TwdlB		3
DRSC23667	2	CG9667	ISY1	0
DRSC03443	1	Ssb-c31a		0
DRSC03036	1	Hsp60C		0
DRSC02832	1	CG5261	DLAT	22
DRSC02921	1	CG6012		0
DRSC06185	1	Tsp42En		0
DRSC07118	1	CG8235	SCYE1	0
DRSC04463	1	mRpS17		0
DRSC07695	1	san	NAT13	0
DRSC06135	1	CG12343	SYF2	0
DRSC07220	1	CG8594	CLCN7	0
DRSC06675	1	GstE5		0
DRSC08307	2	mRpL23	MRPL23	0
DRSC07665	1	plu		0
DRSC08634	1	FucTD		0

DRSC10339	1	CG18769	CCDC109A	0
DRSC23458	2	MED19	MED19	0
DRSC24354	1	CG5389		0
DRSC24518	1	CG6966	FEM1C	0
DRSC24340	1	CG9001		0
DRSC24291	2	ear	MLLT3	0
DRSC25054	1	DebB	SNRPF	2
DRSC24508	2	Hrb98DE	HNRPA1	0
DRSC23350	2	Pcf11		0
DRSC25063	1	mask		0
DRSC25213	2	Rbf	RBL1	0
DRSC23541	2	RnrS	RRM2	0
DRSC23412	3	Rpt3	PSMC4	0
DRSC25607	2	Stam	STAM	0
DRSC25961	3	deltaCOP	ARCN1	0
DRSC23584	2	RpII33	POLR2C	0
DRSC25982	1	RpL6	RPL6	0
DRSC25025	2	RpL22	RPL22	0
DRSC25051	1	RpL37A	RPL37A	0
DRSC23625	3	vih	UBE2C	0
DRSC24322	1	sut3		0
DRSC24141	3	sar1	SAR1B	0
DRSC26043	2	eIF-4a	EIF4A2	0
DRSC26155	1	CG9769	EIF3S5, hCG_15200	0
DRSC26195	3	Ca-P60A	ATP2A1	0
DRSC26313	2	RpS23	RPS23	0
DRSC26257	2	CG13841		0
DRSC26259	2	SmB	SNRPB	0
DRSC08225	1	CG12017		4
DRSC10235	1	CG16998		0
DRSC10896	1	mRpL2	MRPL2	0
DRSC10399	1	CG4098	NUDT9	0
DRSC09778	1	vih	UBE2C	3
DRSC15443	1	CG31473		1
DRSC12307	1	Xe7	CXYorf3	0
DRSC16245	1	Ctr1B		0
DRSC14531	1	dpr4		3
DRSC16827	1	Rlc1	MRPL47	0
DRSC16393	1	CG8165	JMJD1B	1
DRSC16611	2	CoVa	COX5A	0
DRSC15678	1	mRpL9	MRPL9	1
DRSC15582	1	CG4459		0
DRSC15606	1	ire-1	ERN1	0
DRSC17018	1	nos		26
DRSC26217	2	RpL11	RPL11	0
DRSC26226	2	brm	SMARCA4	0
DRSC26265	1	CG17752		0
DRSC26038	1	Cwc25	CCDC49	0
DRSC26371	1	CG8765		0

DRSC26396	2	Nup154	NUP155	0
DRSC27099	2	CG33854	HIST1H3I	0
DRSC26988	1	RpL10Ab	RPL10A	0
DRSC26990	1	mip130	LIN9	0
DRSC27324	1	l(2)NC136	CNOT3	0
DRSC27177	2	Rpn9	PSMD13	0
DRSC27185	2	cul-4	CUL4B	0
DRSC28104	3	CG6015	CDC40	0
DRSC27945	1	CG4119		0
DRSC27971	1	Pop2	CNOT7	0
DRSC27980	2	mor	SMARCC2	0
DRSC28422	2	cact	NFKBIA	0
DRSC28348	2	Hel25E	BAT1	0
DRSC28468	2	RpS7	RPS7	0
DRSC28510	2	RpLP2	RPLP2	0
DRSC28442	2	tomboy40		0
DRSC28396	2	CG1957	CPSF2	1
DRSC28412	1	RpS24	RPS24	0
DRSC28481	2	eIF3-S10	EIF3S10	0
DRSC28414	1	CG3281		0
DRSC28431	2	Tao-1	TAOK1	0
DRSC28523	1	Arpc3B		0
DRSC28871	1	CG32666	STK17A	0
DRSC28833	3	RpL7A	RPL7A	0
DRSC28784	2	RpII18	POLR2F	0
DRSC28626	1	tho2	THOC2	0
DRSC28794	2	sima		0
DRSC28822	2	dalao	SMARCE1	0
DRSC28874	1	ine		0
DRSC28927	1	Corin		0
DRSC28920	1	Ocho		0
DRSC29087	3	CG30382	PSMA6	0
DRSC29116	1	pnt		0
DRSC29232	2	MED7	CRSP9	0
DRSC16590	1	CG9996	GLT8D4	0
DRSC14436	1	CG11910		0
DRSC16028	1	CG6364	UCK2	0
DRSC16326	1	CG31038		3
DRSC18560	1	Unc-76	FEZ2	3
DRSC18382	1	CG4857		2
DRSC18686	1	ND75	NDUFS1	0
DRSC18355	1	Sas10	SAS10	0
DRSC17886	1	CG16752		0
DRSC18368	1	CG4557	TMF1	3
DRSC19778	1	CG32666	STK17A	80
DRSC19355	1	CG10362	PDZD8	7
DRSC19359	1	CG10617	SYT12	0
DRSC19425	1	CG34348	TMEM68	0
DRSC29245	1	hkl		0

DRSC29264	1	Caps	CADPS	0
DRSC29097	1	CG5151		0
DRSC29153	1	CG9507		0
DRSC29315	2	ps	NOVA1	0
DRSC29393	1	Elongin-C	TCEB1	0
DRSC29510	1	mRpL16	MRPL16	0
DRSC29504	2	ncm	KIAA1604	0
DRSC29337	3	CG5245	LOC91664	0
DRSC29362	2	CG1244		0
DRSC29538	1	CG3016	USP30	0
DRSC29851	3	Rab1	RAB1A	0
DRSC30020	1	CG33885	HIST1H4A	0
DRSC29794	1	geminin		0
DRSC29787	1	l(2)08717		0
DRSC29803	2	sbr	NXF1	0
DRSC29772	3	Nup358		0
DRSC29872	1	CG17168		0
DRSC29897	3	Mov34	PSMD7	0
DRSC29905	2	RpL8	RPL8	0
DRSC30026	3	MED30	THRAP6	0
DRSC29708	1	CG8241	DHX8	0
DRSC29702	2	Snx6	SNX6	0
DRSC03080	2	Pvr		0
DRSC03355	1	Kr-h1		12
DRSC00612	2	CG3542	PRPF40A	0
DRSC03574	2	mts	PPP2CB	0
DRSC03419	1	RpS13	RPS13	1
DRSC00267	2	MED15	PCQAP	46
DRSC00619	3	CG3605	SF3B2	0
DRSC03328	3	Fs(2)Ket	KPNB1	2
DRSC03629	1	und	METAP2	0
DRSC02551	1	CG16974		2
DRSC02071	1	CG10570		1
DRSC02179	2	ncm	KIAA1604	1
DRSC01991	1	CG31705		1
DRSC03437	2	SmB	SNRPB	1
DRSC01936	1	CG4891		1
DRSC02161	1	JhI-21	SLC7A5	1
DRSC03569	2	me31B	DDX6	0
DRSC03432	2	Syx5	STX5	0
DRSC03201	3	Pomp		1
DRSC03415	2	RpII33	POLR2C	1
DRSC04456	2	CG4266	SFRS15	0
DRSC18205	1	CG2111		1
DRSC19354	1	CG10353	TMEM16B	1
DRSC19746	1	Pde9		0
DRSC20357	1	nonA	SFPQ	3
DRSC20112	1	CG8565		0
DRSC19984	1	Rad51D		1

DRSC19452	1	CG33173		0
DRSC10087	1	fz2	FZD8	3
DRSC21461	1	Ten-a	ODZ1	9
DRSC21562	1	Dscam	DSCAML1	0
DRSC04053	1	CG10080	VPRBP	0
DRSC04476	3	CG4589	LETM1	0
DRSC04649	1	RpL19	RPL19	1
DRSC04600	3	Ca-P60A	ATP2A1	1
DRSC04908	2	l(2)NC136	CNOT3	2
DRSC04478	1	CG4612		0
DRSC04285	1	key		0
DRSC06805	1	CG30496	GLMN	0
DRSC06803	1	CG1942		0
DRSC07516	3	Prosalpha7	PSMA3	1
DRSC07007	1	CG6701		0
DRSC07442	1	Hsc70-5	HSPA9	2
DRSC07515	3	Prosalpha6	PSMA6	1
DRSC06794	3	Not1	CNOT1	0
DRSC07533	1	RnrS	RRM2	1
DRSC07169	2	RpS23	RPS23	1
DRSC07541	3	Rpn6	PSMD11	0
DRSC07477	2	Nacalpha	NACA	2
DRSC07120	1	CG8241	DHX8	1
DRSC07293	1	prp8	PRPF8	0
DRSC07249	2	CG11198	ACACA	0
DRSC07243	2	cul-4	CUL4B	0
DRSC07696	2	spt4	SUPT4H1	0
DRSC07128	2	l(2)k05713	GPD2	0
DRSC07537	2	RpL11	RPL11	2
DRSC07036	1	CG7744		0
DRSC07659	3	pAbp	PABPC1	0
DRSC08154	3	CG1017	MFAP1	2
DRSC08370	3	CG13900	SF3B3	0
DRSC07302	1	CG8963	PAIP1	53
DRSC07514	3	ProsMA5	PSMA5	0
DRSC08706	3	alphaCop	COPA	0
DRSC08577	2	CG6905	CDC5L	0
DRSC07000	2	Bap55	ACTL6B	0
DRSC11257	3	Prosbeta2	PSMB7	0
DRSC10537	2	Pop2	CNOT7	1
DRSC11112	3	Cdc27	CDC27	1
DRSC09772	1	CG10671	C20orf142	1
DRSC11014	2	MED4	MED4	3
DRSC08207	2	CG11594	FLJ10986	0
DRSC11270	2	RpS12	RPS12	0
DRSC11124	2	CycT	CCNT1	26
DRSC11755	1	CG4365	HAGH	0
DRSC12162	3	CG1109	WDR33	0
DRSC11632	1	Mes2		1

DRSC10899	2	Tom20	TOMM20	0
DRSC12147	3	CG1078		0
DRSC10516	2	MED19	MED19	28
DRSC12367	2	Rpn5	PSMD12	1
DRSC12365	3	Rm62		2
DRSC10722	1	CG6836		1
DRSC12203	1	CG1236	GRHPR	0
DRSC11274	3	Rpn1	PSMD2	0
DRSC12164	1	Hph	EGLN1	1
DRSC12199	1	CG12170	OXSM	0
DRSC12301	3	CG2097	SYMPK	1
DRSC11223	1	Mipp1		0
DRSC12369	2	Snr1	SMARCB1	0
DRSC12383	3	noi	SF3A3	1
DRSC12387	2	sec23	SEC23A	0
DRSC11256	3	Pros26	PSMB1	0
DRSC12536	3	snRNP2	SNRPD2	1
DRSC10559	3	CG5931	ASCC3L1	0
DRSC11224	1	Mo25	CAB39L	0
DRSC11324	1	asf1	ASF1A	1
DRSC11642	3	Rpb8	POLR2H	0
DRSC11808	2	MED1	PPARBP	0
DRSC11874	2	Pitslre		1
DRSC11634	1	Ssl1	LOC728340	0
DRSC11697	1	CG32428		21
DRSC12567	1	CG33097		10
DRSC14935	3	CG14712	POM121	0
DRSC17077	2	tgo	ARNT	1
DRSC15675	2	ear	MLLT3	7
DRSC17022	2	osa	ARID1A	1
DRSC16639	2	DDB1	DDB1	0
DRSC15741	1	CG5220	FTSJ1	0
DRSC16215	1	CG7215	PRDX5	0
DRSC16109	1	EloA	TCEB3	7
DRSC16889	2	MED17	CRSP6	0
DRSC14384	2	CG11779	TIMM44	0
DRSC16962	2	gro	TLE3	0
DRSC16034	3	Dis3	DIS3	0
DRSC14886	2	CG14542	CHMP2A	2
DRSC16210	1	CG7183	C3orf19	0
DRSC14209	2	Nup98		1
DRSC16882	1	TfIIA-L	GTF2A1	0
DRSC16840	2	Rpn9	PSMD13	1
DRSC16018	2	mask		4
DRSC16208	2	CG7168	COMMD2	0
DRSC15895	2	CG5857	TMEM48	0
DRSC14109	2	Ald		3
DRSC14627	1	CG13625	BUD13	0
DRSC16833	3	RpL4	RPL4	3

DRSC17154	3	CG2165	ATP2B3	0
DRSC18748	1	bys	BYSL	0
DRSC18760	3	deltaCOP	ARCN1	1
DRSC17970	2	l(1)G0155	YKT6	0
DRSC14598	3	Gfat2	GFPT1	1
DRSC18293	2	RpL17	RPL17	5
DRSC14146	2	CG1957	CPSF2	0
DRSC21664	1	plexB	PLXNB1	0
DRSC22614	1	IP3K2		5
DRSC22218	1	betaTub60D	TUBB3	1
DRSC22814	1	CG12817, CG12420		0
DRSC03751	1	CG40169		0
DRSC23118	1	CG16947	RCHY1	2
DRSC21271	1	mt:ND6		1
DRSC23049	1	mei-P26		0
DRSC14168	2	Bub3	BUB3	1
DRSC18755	3	crn	CRNKL1	0
DRSC17012	2	ncd	KIFC1	0
DRSC18835	1	snf	SNRPA	0
DRSC16709	1	Hrb98DE	HNRPA1	2
DRSC17098	2	zfh1	ZEB1	6
DRSC19337	3	Bap60	SMARCD1	0
DRSC19338	3	CG6842	VPS4B	2
DRSC19904	3	Nup153	NUP153	0
DRSC20297	2	U2af50	U2AF2	0
DRSC19786	3	Tango4	PLRG1	1
DRSC18420	1	CG7065		3
DRSC17818	1	CG12123		0
DRSC20229	1	Chc	CLTC	0
DRSC20378	2	sno	SBNO1	0
DRSC20539	2	l(1)G0269	DULLARD	0
DRSC00789	2	Slh	SCFD1	0
DRSC00782	1	RpL40	UBA52	0
DRSC02680	2	CG18591	SNRPE	0
DRSC03463	2	MED20	TRFP	0
DRSC03526	2	eIF-4a	EIF4A2	1
DRSC02739	3	HDC01675		0
DRSC01999	2	Nup107	NUP107	0
DRSC03417	2	RpL7	RPL7, hCG_31916	1
DRSC03421	2	RpS27A	RPS27A	0
DRSC02921	1	CG6012		0
DRSC02876	1	CG5681		2
DRSC02878	2	CG5693		0
DRSC02087	2	RpL30	RPL30	0
DRSC03296	1	CycE	CCNE1	0
DRSC02603	2	CG17331	PSMB2	0
DRSC03420	1	RpS26	RPS26, LOC728937	0
DRSC02668	2	Mio		0
DRSC04312	1	CG18735	LOC646960	2

DRSC04094	1	CG11269		0
DRSC04601	2	Cdk9	CDK9	0
DRSC04191	2	CG13550		2
DRSC03801	3	RpL5		4
DRSC03737	2	Ef2b	EEF2	0
DRSC04559	2	dom		1
DRSC03757	2	CG33870	HIST2H2BF	0
DRSC03704	3	RpL21	RPL21, LOC729402	0
DRSC04648	3	RpL23	RPL23	0
DRSC04987	1	CG3267	MCCC2	0
DRSC04883	1	Nipped-A	TRRAP	0
DRSC06808	1	CSN7	COPS7B	0
DRSC07662	2	phr		0
DRSC04344	2	RpL12		0
DRSC06787	2	Not1	CNOT1	0
DRSC06651	1	CG17050		0
DRSC06797	1	CG1888		0
DRSC07408	3	E(Pc)		0
DRSC07397	3	DebB	SNRPF	6
DRSC07553	3	SmD3	SNRPD3	1
DRSC05953	3	CG8878		0
DRSC07517	3	Prosbeta5	PSMB5	2
DRSC06716	3	RpL31		0
DRSC06371	1	CG13337		1
DRSC07078	1	CG8093	LIPM	0
DRSC06196	1	kn	EBF2	11
DRSC06644	1	CG17034	ATP8A1	0
DRSC07538	3	RpL18A	LOC285053	0
DRSC07151	3	RpS15	RPS15	3
DRSC05998	1	CG10734		0
DRSC07539	3	RpLP2	RPLP2	3
DRSC07519	1	Psi	FUBP1	2
DRSC06900	3	eIF3-S9	EIF3S9	0
DRSC07088	2	dup	CDT1	0
DRSC06675	1	GstE5		0
DRSC08307	2	mRpL23	MRPL23	0
DRSC07665	1	plu		0
DRSC07556	3	Spt5	SUPT5H	0
DRSC08494	1	CG32306		0
DRSC08634	1	FucTD		0
DRSC07423	1	Elongin-C	TCEB1	1
DRSC07583	2	betaTub56D	TUBB2C	4
DRSC07818	2	RpL38		0
DRSC08731	1	pUf68	SIAHBP1	4
DRSC11401	1	tan		0
DRSC10339	1	CG18769	CCDC109A	0
DRSC08225	1	CG12017		4
DRSC10235	1	CG16998		0
DRSC10274	2	mad2	MAD2L1	0

DRSC08183	1	CG11357		0
DRSC10452	2	CG4835		16
DRSC08701	2	TfIIEbeta	GTF2E2	0
DRSC11165	2	Fad2		2
DRSC10696	2	CG6694		1
DRSC11271	1	RpS17	RPS17	0
DRSC10533	2	CG5651	ABCE1	0
DRSC10474	2	MED10	MED10	0
DRSC11341	2	eIF-2beta	EIF2S2	2
DRSC11272	1	RpS4	RPS4X	0
DRSC11330	2	brm	SMARCA4	1
DRSC11412	3	zetaCOP	COPZ1	0
DRSC10489	1	CG5161	TRAPPC2	0
DRSC09800	1	snRNP69D	SNRPD1	1
DRSC11275	3	Rpn12	PSMD8	0
DRSC11222	1	Mi-2	CHD4	2
DRSC11388	2	rept	RUVBL2	1
DRSC11663	2	Spc105R		0
DRSC10912	2	CG7757	PRPF3	0
DRSC10726	2	RpL26	RPL26	0
DRSC11876	3	Pros54	PSMD4	0
DRSC12623	3	alphaTub84D	TUBA3D	3
DRSC17034	2	puc	DUSP10	2
DRSC14371	1	CG31258		1
DRSC16535	1	CG9667	ISY1	2
DRSC12622	2	alphaTub84B	TUBA1A	3
DRSC11947	2	Qm		0
DRSC14531	1	dpr4		3
DRSC16827	1	Rlc1	MRPL47	0
DRSC16393	1	CG8165	JMJD1B	1
DRSC16611	2	CoVa	COX5A	0
DRSC16433	1	RpS29	RPS29	0
DRSC15147	2	CG33936	ZFAND6	0
DRSC16555	1	bel	DDX3X	4
DRSC16899	3	alphaTub85E	TUBA1C	4
DRSC14573	1	CG12945		0
DRSC16493	1	CG9444		0
DRSC17029	1	pont	RUVBL1	0
DRSC16834	2	RpL3	RPL3	0
DRSC16388	1	ps	NOVA1	1
DRSC15678	1	mRpL9	MRPL9	1
DRSC16387	1	CG8141		0
DRSC16231	1	btsz		0
DRSC16940	3	eff	UBE2D3	0
DRSC15119	2	RpS30	FAU	1
DRSC17018	1	nos		26
DRSC14708	1	CG13858		0
DRSC16291	1	CG7698	CPSF3	1
DRSC15804	2	snRNP-U1	SNRPC	0

DRSC16836	1	RpS20	RPS20	0
DRSC16937	2	eIF-1A	EIF1AX	0
DRSC16808	2	Rab1	RAB1A	1
DRSC15687	2	CG4963	SLC25A37	0
DRSC17091	1	ttk		18
DRSC16984	1	larp		9
DRSC16321	1	CG7824		0
DRSC16973	1	janB		0
DRSC14742	2	CG14247		4
DRSC15691	2	Mes-4	WHSC1	0
DRSC16326	1	CG31038		3
DRSC17194	1	ATPsyn-beta	ATP5B	0
DRSC17731	2	tlk		1
DRSC18646	1	CG3708		0
DRSC18382	1	CG4857		2
DRSC17920	1	CG14423		5
DRSC18184	2	crn	CRNKL1	3
DRSC18091	2	CG15785		0
DRSC18368	1	CG4557	TMF1	3
DRSC18006	3	CG15321		11
DRSC18686	1	ND75	NDUFS1	0
DRSC18355	1	Sas10	SAS10	0
DRSC17886	1	CG16752		0
DRSC18750	1	c12.1	HSPC148	6
DRSC18347	2	RpL35	RPL35	0
DRSC18241	1	CG2909		0
DRSC18666	2	Gclc	GCLC	0
DRSC19831	2	RpS15Ab		0
DRSC20368	2	sbr	NXF1	1
DRSC06831	3	CG2249		0
DRSC19372	1	CG34346		4
DRSC11632	2	Mes2		1
DRSC16835	2	RpL32	RPL32	1
DRSC22145	2	RpLP1	RPLP1	21
DRSC22323	2	RpL18	RPL18	0
DRSC22359	3	polo	PLK1	2
DRSC21625	1	Klp3A	KIF4A	0
DRSC22614	1	IP3K2		5
DRSC22218	1	betaTub60D	TUBB3	1
DRSC22723	1	CG31246		34
DRSC22110	2	RpLP0	RPLP0	0
DRSC22071	2	snRNP70K	SNRP70	1
DRSC22667	2	CG9775		0
DRSC22926	2	tlk		0
DRSC22794	1	pum	PUM2	0
DRSC22819	2	RpL22	RPL22	8
DRSC23111	2	Tbp	TBP	0
DRSC01413	1	CG31775		92
DRSC23091	1	MED11		1

DRSC36563	1	CR32477	0
DRSC23240	1	msopa	0

Table S2. List of genes in secondary screen.

Amplicon	Alternative amplicon tested	Gene \Flybase_ID	Human Homologene	of Interest
DRSC22061	DRSC39837	olf186-F	TMEM142A	3
DRSC20158	DRSC39682	Stim	STIM1	3
DRSC26195	DRSC26195	Ca-P60A	ATP2A1	3
DRSC17154	DRSC38802	CG2165	ATP2B3	3
DRSC04476	DRSC36117	CG4589	LETM1	3
DRSC18796		Tom40	TOMM40	3
DRSC28442	DRSC28442	tomboy40		2
DRSC14384	DRSC33250	CG11779	TIMM44	2
DRSC10899	DRSC39868	Tom20	TOMM20	2
DRSC02774	DRSC34518	CG4738	NUP160	2
DRSC07129		CG8257	CARS2	
DRSC29510	DRSC29510	mRpL16	MRPL16	1
DRSC12301	DRSC32363	CG2097	SYMPK	3
DRSC08721	DRSC34572	mge	TOMM22	3
DRSC19338	DRSC31082	CG6842	VPS4B	3
DRSC11330	DRSC30901	brm	SMARCA4	2
DRSC28422	DRSC30704	cact	NFKBIA	2
DRSC28822	DRSC35681	dalao	SMARCE1	
DRSC29504	DRSC31772	ncm	KIAA1604	1
DRSC29315	DRSC29574	ps	NOVA1	
DRSC29851	DRSC33339	Rab1	RAB1A	2
DRSC03574	DRSC30716	mts	PPP2CB	2
DRSC29362	DRSC32828	CG1244		2
DRSC03569	DRSC38084	me31B	DDX6	2
DRSC10516	DRSC30863	MED19	MED19	2
DRSC12387	DRSC31247	sec23	SEC23A	1
DRSC14109	DRSC31420	Ald	aldolase A	2
DRSC17022	DRSC33079	osa	ARID1A	2
DRSC16133	DRSC39065	Fer3	FERD3L	2
DRSC16150	DRSC35466	Nup133	NUP133	2
DRSC16711	DRSC32138	Hsc70-4		1
DRSC16810	DRSC31657	Rab7	RAB7A	2
DRSC17997	DRSC27473	CG1531		
DRSC18116		CG1677	NHN1	3
DRSC03463	DRSC33063	MED20	TRFP	2
DRSC06644	DRSC06644	CG17034	ATP8A1	1
DRSC10533	DRSC32078	CG5651	ABCE1	2
DRSC07955	DRSC31917	CG7971	SRRM2	2
DRSC17638	DRSC31031	Hk	KCNAB1	
DRSC05050	DRSC33652	CG11166		
DRSC13664	DRSC30941	nAcRalpha-96Aa	CHRNA3	2
DRSC23615	DRSC32150	MED15	PCQAP	1
DRSC28179	DRSC30824	Klp61F	KIF11	2
DRSC03492		beta'Cop	COPB2	2
DRSC30006	DRSC30006	CG15609	EHBP1	
DRSC23203	DRSC33101	sima		2

DRSC20283	DRSC32209	Rpt3	PSMC4	3
DRSC23578	DRSC34254	desat1		3
DRSC24497	DRSC24497	CG17751		1
DRSC24015	DRSC34556	Hsc70-5	HSPA9	1
DRSC03036	DRSC29438	Hsp60C		1
DRSC21247	DRSC34562	Hsp70Bb	Hsp70Bb	1
DRSC25052		Hsp83		1
DRSC25105	DRSC33319	Hsc70-3	HSPA5	2
DRSC25108	DRSC32144	lark	RBM4B	2
DRSC02161	DRSC29181	JhI-21	SLC7A5	
DRSC28394	DRSC31394	Pp2A-29B	PPP2R1A	2
DRSC26676	DRSC35320	CG4196	TMEM165	
DRSC03444	DRSC37259	Stam	STAM	2
DRSC03384	DRSC34700	Nup154	NUP155	2
DRSC04456		CG4266	SFRS15	2
DRSC12147	DRSC33611	CG1078		3
DRSC14935	DRSC31781	CG14712	POM121	3
DRSC15675	DRSC37978	ear	MLLT3	2
DRSC16210		CG7183	C3orf19	
DRSC16208	DRSC36275	CG7168	COMMD2	
DRSC17049	DRSC31665	sar1	SAR1B	3
DRSC15895	DRSC39536	CG5857	TMEM48	2
DRSC26038	DRSC35049	CG2843	CCDC49	
DRSC16005	DRSC32492	mask	ANKHD1	1
DRSC17012	DRSC36317	ncd	KIFC1	2
DRSC18704	DRSC35979	Rbf	RBL1	2
DRSC17741	DRSC35318	CG4119		
DRSC17755	DRSC24030	CG10777	DDX17	2
DRSC20539		l(1)G0269	DULLARD	2
DRSC05953	DRSC31940	CG8878		3
DRSC03356	DRSC39752	Kr-h2	TMEM33	
DRSC14893	DRSC34020	CG14550		1
DRSC15687	DRSC34889	CG4963	SLC25A37	2
DRSC18750	DRSC31704	c12.1	HSPC148	1
DRSC20576	DRSC31173	cactin	C19orf29	
DRSC20904	DRSC29872	CG17168	SNIP1	1
DRSC13916		ligatin	LGTN	
DRSC19425	DRSC19644	CG34348	TMEM68	
DRSC23135	DRSC30026	MED30	THRAP6	2
DRSC10512		PGRP-L	TMEM11	
DRSC25280	DRSC35474	CG7065		
DRSC10339		CG18769	CCDC109A	
DRSC25351	DRSC25351	Nacalpha	NACA	1
DRSC23629	DRSC23629	Kr-h1		1
DRSC19354	DRSC29888	CG10353	TMEM16B	
DRSC26948	DRSC35756	Gfat2	GFPT1	3
DRSC27224	DRSC40402	CG13865		2
DRSC27645	DRSC27645	CG12702		
DRSC27581	DRSC32165	Pomp		2
DRSC28779	DRSC33488	Bub3	BUB3	2

DRSC29772	DRSC34581	Nup358		2
DRSC29930	DRSC37262	tgo	ARNT	1
DRSC29013	DRSC29013	bys	BYSL	
DRSC01999	DRSC34579	Nup107	NUP107	2
DRSC09772	DRSC28750	CG10671	C20orf142	
DRSC00533	DRSC40282	CG2789		
DRSC00520	DRSC35011	CG18317	SLC25A36	
DRSC08679	DRSC40381	Mtch		
DRSC16351		CG7943	MCART2	
DRSC20125	DRSC39802	CG8931	SLC25A46	
DRSC02888		CG5755		
DRSC07337		CG9090	SLC25A3	
DRSC10742	DRSC35463	CG6893		
DRSC15145	DRSC34173	CG16736		
DRSC15761	DRSC39880	CG5281		
DRSC14476	DRSC33788	CG12201	SLC25A22	
DRSC15636	DRSC40276	CG4743	SLC25A26	
DRSC15687	DRSC34889	CG4963	SLC25A37	2
DRSC17765		CG10920		
DRSC19565	DRSC19565	Shawn	SLC25A40	
DRSC19565	DRSC19565	Tyler		
DRSC17440	DRSC39375	vanin-like		
DRSC27826	DRSC27826	porin	VDAC2	
DRSC29490	DRSC30967	CG6608		
DRSC25627	DRSC35013	CG18347		
DRSC29759	DRSC29759	CG5646		
DRSC24316	DRSC24316	CG2616		
DRSC00808	DRSC29025	colt	SLC25A20	
DRSC02714	DRSC39544	CG3476		
DRSC02801		CG4995	SLC25A29	
DRSC06721	DRSC26600	CG18324		
DRSC08535	DRSC25732	CG18418	SLC25A11	
DRSC10293	DRSC34381	CG32103	SLC25A24	
DRSC11261	DRSC31659	Rab8	RAB8A	
DRSC16114	DRSC40350	CG6782	SLC25A1	
DRSC14125	DRSC35572	CG8790	SLC25A10	
DRSC15561	DRSC24659	CG4323		
DRSC15399	DRSC40303	CG1907		
DRSC18109		CG1628	SLC25A15	
DRSC20625	DRSC27260	CG14613		1
DRSC03267		CG9582		
DRSC04322	DRSC40008	CG2857		
DRSC06058		CG11196		
DRSC07056	DRSC40234	CG8026	SLC25A32	
DRSC07149	DRSC35542	CG8323	SLC25A34	
DRSC06722	DRSC39345	CG18327		
DRSC08597	DRSC25670	CG7514	SLC25A11	
DRSC10317	DRSC35014	CG18363		
DRSC15556		CG4241	SLC25A42	
DRSC18611		CG5254	SLC25A21	

DRSC20371	DRSC34592	sesB	SLC25A6	
DRSC21939	DRSC39444	CG32250	SLC25A17	
DRSC25670	DRSC25670	CG7514		
DRSC27260	DRSC27260	CG14613		1

Table S3. List of candidate genes.

Amplicon #1	Amplicon #2	Of Interest	Gene\Flybase_ID	Human Homologene
DRSC04476	DRSC36117	3	CG4589	LETM1
DRSC15687	DRSC34889	2	CG4963	SLC25A37
DRSC29504	DRSC31772	2	ncm	KIAA1604
DRSC07477	DRSC25351	2	Nacalpha	NACA
DRSC25213	DRSC35979	2	Rbf	RBL1
DRSC24291	DRSC37978	2	ear	MLLT3
DRSC25105	DRSC33319	2	Hsc70-3	HSPA5
DRSC20967	DRSC40402	2	CG13865	
DRSC29362	DRSC32828	2	CG1244	
DRSC05050	DRSC33652	2	CG11166	